

Discovery prospects with the Dark-photons & Axion-Like particles Interferometer

Javier De Miguel^{1,2,3,*}, Juan F. Hernández-Cabrera^{2,3}, Elvio Hernández-Suárez^{2,3}, Enrique Joven-Álvarez^{2,3}, Chiko Otani¹, and J. Alberto Rubiño-Martín^{2,3}

¹*The Institute of Physical and Chemical Research (RIKEN),*

Center for Advanced Photonics, 519-1399 Aramaki-Aoba, Aoba-ku, Sendai, Miyagi 980-0845, Japan

²*Instituto de Astrofísica de Canarias, E-38200 La Laguna, Tenerife, Spain and*

³*Departamento de Astrofísica, Universidad de La Laguna, E-38206 La Laguna, Tenerife, Spain*

On behalf of the DALI Collaboration

(Dated: January 11, 2024)

We discuss the discovery potential of the Dark-photons & Axion-Like particles Interferometer (DALI) in this letter. The apparatus, currently in a design and prototyping phase, will probe axion dark matter from the Teide Observatory, an environment protected from terrestrial microwave sources, reaching Dine–Fischler–Srednicki–Zhitnitsky-like axion sensitivity in the range 25–250 μeV of mass. The experimental approach shows also a potential to probe dark sector photons of kinetic mixing strength in excess of several 10^{-16} ; and to establish new constraints to a stochastic gravitational wave background in its band. We identify different branches, including cosmology, stellar and particle physics, where this next-generation halo-telescope may play a role in coming years.

I. INTRODUCTION

Non-luminous, ‘dark’ matter is thought to play a role in galactic dynamics, the halos of spiral galaxies being benchmark astronomical laboratories [1–3]. In parallel, the current picture in cosmology suggests that a cosmological constant, Λ , and cold dark matter (CDM), enormously influence the evolution of the universe. A highly accelerated inflationary expansion during a brief cosmological timeframe, and the cosmic microwave background (CMB), also shape the Λ CDM model [4–10]. Large scale observations, simulations and the anisotropy measured in the CMB seem agreed in indicating the existence of CDM to favour the formation of the structures observed in the contemporary Cosmos [11–23].

The quantum chromodynamics (QCD) axion is a long-postulated pseudo-scalar boson that arises as a consequence of the dynamic solution to the charge and parity (CP) symmetry problem in the strong interaction [24–26]. Furthermore, axion can simultaneously solve the dark matter enigma in a broad coupling strength to photons, $g_{a\gamma\gamma}$, to axion mass, m_a , parameter space [27–30]. Moreover, beyond shaping galaxies by forming halos, the primordial density perturbations from which galaxies evolved may have been produced by the presence of temporary axion domain walls in the early Universe [31]. Indeed, approaches have been proposed that simultaneously solve the strong CP problem, axion dark matter and inflation in an unique model [32–36]. On the other hand, astronomical observations and simulations have given rise to the conjecture that dark matter in the nearby Universe is distributed in the form of substructures [37–43]. Lastly, a series of anomalous astronomical

observations have led to hypothesize that new physics may play a role in stellar evolution [44–47].

All of the above encourages the quest for axion dark matter. The search for dark matter by axion-photon interaction is promising. Laboratory experiments have excluded the sector $g_{a\gamma\gamma} \gtrsim 10^{-7} \text{ GeV}^{-1}$ for $m_a \lesssim 10^{-3} \text{ eV}$ [48–51]. Helioscopes, partially overlapping stellar hints based on interactions of the axion to standard particles in the plasma of stars, exclude $g_{a\gamma\gamma} \gtrsim 10^{-10} \text{ GeV}^{-1}$ for $10^{-2} \lesssim m_a/\text{eV} \lesssim 10^5$ [52]. Different astronomical campaigns and simulations rule out distinct parameter spaces [53–58]; while cosmology also restricts the mass of this pseudo-Goldstone boson to allow the structures observed in the contemporary Universe to be formed in a CDM picture and, as a result, the search for axion in the range $10^{-6} \lesssim m_a/\text{eV} \lesssim 10^{-3}$ is well motivated [30, 59].

The velocity dispersion of Halo dark matter is about $10^{-3}c$, with c the speed of light. Therefore, the dynamic mass and the rest mass of these axions approximately coincide. The wavelength of the electromagnetic radiation emitted by axion-to-photon conversion is $\omega \sim m_a$. Axion haloscopes [60] are magnetised detectors that probe Galactic dark matter via the inverse Primakoff effect [61]. This is the experimental approach to which we will confine our attention throughout this work; which is also sensitive to the dark photon via kinetic mixing [62, 63], and to high-frequency gravitational waves, within a faint parameter space determined by the Planck scale, through photon-graviton oscillation in an external magnetic field [64–69].

The rest of this letter is structured as follows. In Sec. II we overview the experimental setup of DALI Experiment. Section III is devoted to examine its discovery potential. Conclusions are drawn in Sec. IV.

* javier.miguelhernandez@riken.jp

II. EXPERIMENTAL APPROACH

The quest for axion at masses below a few dozen microelectronvolt has been performed by haloscopes for decades [70–75]. Unfortunately, the search for axion at ‘high frequency,’ above, say, two dozen microelectronvolt of mass or, equivalently, about half a dozen gigahertz, remains poorly explored. In the Sikivie cavity-haloscope principle, the signal power originating from axion-to-photon conversion scales as $P \propto g_{a\gamma\gamma}^2 B_0^2 V C Q_L \rho_a / m_a$ —e.g., [71]. Here, B_0 is magnetic field strength; V is the volume; C is the form factor; Q_L is the loaded quality factor and ρ_a is the local density of axion dark matter, which saturates at $\sim 1/2 \text{ GeV cm}^{-3}$ [3]. The resonant frequency scales inversely on the cavity size, or the distance between the movable rods used for tuning, in the form $\nu_0 \sim c/d$; d being the diameter or distance. Smaller cavities provide a smaller detection volume which results in a lower signal power. Together with hurdles such as misalignment and sticking of the rods, radiation leakage as a result of external mechanical tuning, poor rod thermalisation, skin effect, etc., this can degrade the scanning speed at higher frequencies—e.g., see [76, 77]. In contrast, DALI [78–80] incorporates a multi-layer Fabry–Pérot resonator [81] instead of a closed resonant cavity, or rather than superconducting wire planes as proposed by Sikivie [60, 82, 83]. In a dielectric Fabry–Pérot axion haloscope, the plate area, A , is decoupled from the resonant frequency, provided its size is larger than the scanning wavelength to avoid diffraction, enabling access to heavier axions. A similar concept is being developed by other collaborations, including MADMAX, ADMX-Orpheus, LAMPOST, MuDHI or DBAS [84–92].

In the DALI interferometer, constructive interference is caused by reflection off a top mirror, originating a standing wave. The resonant frequency is tuned by setting a plate distance of a fraction of the scanning wavelength, typically $\sim \lambda/2$ with a plate thickness of $\sim \lambda/(2\sqrt{\epsilon_r})$ in a half-wavelength stack. However, the resonance is periodic over $\sim 4\nu_0$ intervals [93, 94]. A one-eighth wavelength configuration allows the plate distance to be shortened by about four times to probe a desired frequency range. Therefore, a $\sim \lambda/8$ spacing is to be used at lower frequencies in order to save room inside the magnet bore, while the usual $\sim \lambda/2$ configuration can be employed at higher frequencies—cf. [79, 95, 96] for a proof of concept. Furthermore, multiple axion masses, about four wavelengths distant, could be probed simultaneously by alternating receivers centered at different frequencies on the focal plane of the haloscope without significantly decreasing its performance, in analogy with CMB experiments to which we have contributed—e.g., [97–100]. Once implemented, this multi-frequency approach would double the scanning speed of the haloscope with respect to the numbers that we will adopt throughout this article. The quality factor, Q , is the signal power enhancement over a narrow bandwidth centered at a resonant frequency. The group delay time, τ_g , is the average lifetime of a photon

within each volume enclosed between two adjacent reflectors, $\tau_g = -d\phi/d\omega$; ϕ being the phase. The quality factor of a Fabry–Pérot resonator is $Q = \omega\tau_g$; with ω the angular frequency [93].¹ The Q factor scales linearly with the number of layers in series [79, 101]. A higher electric permittivity, ϵ_r , results in a higher Q and a narrower full width at half maximum of the spectral feature caused by autocorrelation. The signal originating from axion-to-photon conversion is weak. The quality factor necessary to achieve QCD axion sensitivity, $Q \sim 10^4$, is tenable over a bandwidth of several dozens of megahertz at frequencies of tens of gigahertz [78, 79]. The error budget in plate spacing is set to a fraction of a few hundredths of the scanning wavelength by means of electromagnetic finite elements method simulations with adaptive mesh refinement [102]. In consequence, the experimental range of DALI extends up to approximately 250 μeV axion mass. Over broad bands, the experiment requires reconfiguration. This reconfiguration involves replacing receivers every few gigahertz, mechanical tuner components, and other accessories. Taking into account a scan speed of a few GHz per year, this reconfiguration is planned every several years as a part of a scientific program that would extend over more than a decade. The DALI concept is shown in Fig. 1, and detailed in depth in [78].

In DALI, the signal power induced by axion scales as $P \propto g_{a\gamma\gamma}^2 B_0^2 A Q \rho_a / m_a^2$. A highly sensitive DALI instrument requires to maximize the cross-sectional area of detection, A , via a large magnet bore; the power enhancement factor, Q , and, crucially, the external field strength, B_0 , by incorporating a potent superconducting magnet. Niobium–titanium, NbTi, superconductor does not provide magnetic field flux densities above 9–10 T when cooled down to a physical temperature of 4.2 K. However, using more powerful, and demanding, cryogenic systems, NbTi can be cooled down to 2 K, which makes field strengths of up to about 11.7 T frequent [109–111]. Therefore, regular multicoil magnets and solenoids present field strengths of 9.4 or 11.7 T with a warm bore of about 50–90 cm, from a few to several meters in length, and a field homogeneity of several dozens parts per million over a few centimeters diameter of spherical volume. In occasions, niobium–tin, Nb_3Sn , is used to provide field strengths beyond 11.7 T, with an upper limit of approximately 23.5 T. However, this superconductor material is, roughly, one order of magnitude more costly than NbTi and, therefore, its use is less widespread. Finally, high-temperature superconductors have been proposed to reach magnetic fields in excess of 23.5 T, although they are still at an early stage of development, while hybrid magnets that far surpass the state of the art are also maturing. Solenoids and multicoil superconducting magnets are employed in magnetic res-

¹ The power boost factor as defined by MADMAX and the quantum optics definition of the quality factor are equivalent in a transparent mode.

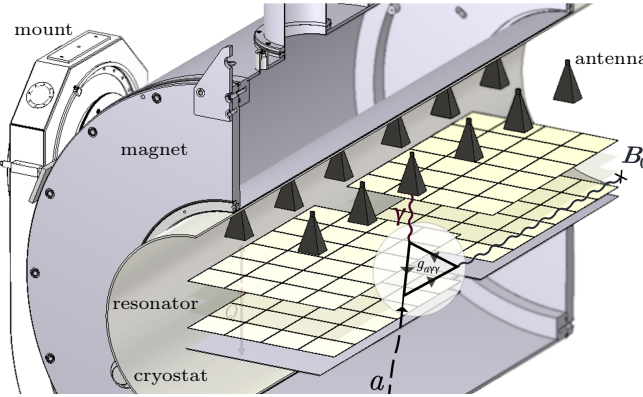


FIG. 1. DALI concept. The experiment cryostat, cylindrical shape, is housed within the warm bore of a solenoid superconducting magnet and employs an independent ^3He cooling system which provides a sub-kelvin background temperature. The ceramic layers, in yellow, consist of a grid of wafers of a good dielectric material, e.g. zirconia (ZrO_2). Zirconia is a robust ceramic distributed in a range of thicknesses that has a high dielectric constant, up to $\epsilon_r \gtrsim 40$, and a low loss tangent, of the order of $\tan \delta \sim 10^{-4}$ at $\mathcal{O}(10)$ GHz frequencies [96, 103]. A polished mirror is attached at the bottom to envelop the Fabry-Pérot interferometer. The signal enhancement over a narrow bandwidth centered at a resonant frequency is the quality factor, Q . The microwave signal, originating at an axion-photon-photon vertex, is received by an antenna array, in black. This array of receivers is housed inside the same experiment cryostat with the field lines aligned with the high electron mobility transistors to cancel spurious effects [104–106]. The data acquired from different channels are post-processed and combined using techniques similar to radio interferometry that we have developed over decades of CMB observations—e.g., [97–100]. This tool allows for calibration, correction of phase mismatch and compensate for differences between pixels, etc., with a negligible error [107, 108]. This setup allows for a larger cross-sectional area inside a regular solenoid-type magnet. The apparatus rests on an altazimuth mount, in white on the left, to provide the instrument with additional directional sensitivity. The overall dimensions are a few meters in length and about one meter in diameter. Some components have been removed for simplicity.

onance imaging (MRI), industry and research [109–111]. DALI is designed to employ a regular MRI-type magnet with a high field stability and ultra high homogeneity, at the level of $<1\%$ inhomogeneity over a 100 mm diameter sphere, thereby ensuring a constant field density in the volume destined to enclose the instrument; which can operate in multiple positions. An initial, cost-effective phase using a NbTi superconducting magnet operating at ~ 4 K to provide a ~ 9 T field is planned for the DALI Experiment, which we will refer to as ‘phase I.’ A second phase, with a higher scan speed, is an up-grade to ~ 11.7 T using a larger magnet working at ~ 2 K. In both phases of the project only currently available technology is to be used as part of a strategy to contribute an experiment with feasibility and readiness. Note, the phase I configuration would also allow the search for DFSZ I

axions up to ~ 250 μeV , although this would multiply by a factor of about twenty the time required to probe a band at a given confidence level.

III. DISCOVERY POTENTIAL

In this section we look at the potential of DALI to unveil new physics.

A. CP symmetry and axion dark matter

The QCD Lagrangian density includes an angular term, which is read

$$\mathcal{L}_\theta = \frac{1}{32\pi^2} \theta G_{\mu\nu}^a \tilde{G}_{\mu\nu}^a, \quad (1)$$

where the gluon field strength is $G_{\mu\nu}^a$ and $\tilde{G}_{\mu\nu}^a$ its dual. We express natural units throughout this letter, except where indicated explicitly. In the most natural explanation to date, CP symmetry is preserved in QCD since the θ term in Eq. 1, which allows for symmetry violation, is promoted to a field with a Mexican hat potential that evolves towards a minimum as time advances in an early Universe [24]. Oscillations give rise to particles, which have been termed ‘axion’ [25, 26]. The non-observation of a neutron electric dipole moment by modern experiments suggest that θ is negligibly small and, consequently, CP symmetry would be preserved, in practice, at present [112, 113]. Axion interacts weakly with Standard Model particles. The axion-photon interaction term is

$$\mathcal{L}_{a\gamma}^{\text{int}} = -\frac{1}{4} g_{a\gamma} F_{\mu\nu} \tilde{F}^{\mu\nu} a, \quad (2)$$

with $F^{\mu\nu}$ the photon field strength tensor and a the axion field. From a classic approach, Eq. 2 simplifies to $\mathcal{L}_{a\gamma}^{\text{int}} = g_{a\gamma} \mathbf{E} \cdot \mathbf{B} a$; \mathbf{E} being the photon field and \mathbf{B} a static magnetic field that contributes a virtual photon which enables the Primakoff effect at an axion-photon-photon vertex, $a + \gamma_{\text{virt}} \leftrightarrow \gamma$ [61].

The coupling rate of the QCD axion contains a factor derived from the ratio of electromagnetic and color anomalies, \mathcal{E}/\mathcal{C} , which reads $c_{a\gamma\gamma} = 1.92(4) - \mathcal{E}/\mathcal{C}$; with $c_{a\gamma\gamma} = -\frac{\alpha}{2\pi} g_{a\gamma\gamma} f_a$, α being the fine structure constant and f_a the axion field scale—giving the digit in parentheses accounts for the uncertainty. In the Kim–Shifman–Vainshtein–Zakharov (KSVZ) model, $\mathcal{E}/\mathcal{C} = 0$ and $\mathcal{C} = 1$ are adopted [114, 115]. In contrast, the Dine–Fischler–Srednicki–Zhitnitsky (DFSZ) axion adopts \mathcal{E}/\mathcal{C} equal $8/3$ —the so-called DFSZ I—or $2/3$ —DFSZ II—and \mathcal{C} equal to 6 or 3 [116, 117]. Differently from QCD axion models, for the so-called axion-like particles (ALPs), which arise in extensions of the Standard Model of particle physics, coupling to photons and mass are uncou-

pled, resulting in a larger parameter space to be explored [118, 119].

The core objective of DALI is to detect Galactic axion dark matter. The haloscope is sensitive to axion-like particles with a coupling strength to photons of [78]

$$\begin{aligned} \frac{g_{a\gamma\gamma}}{\text{GeV}^{-1}} &\gtrsim 2.7 \times 10^{-13} \times \left(\frac{\text{SNR}}{Q} \right)^{1/2} \\ &\times \left(\frac{m^2}{A} \right)^{1/2} \times \left(\frac{m_a}{\mu\text{eV}} \right)^{5/4} \times \left(\frac{1\text{s}}{t} \right)^{1/4} \\ &\times \left(\frac{T_{\text{sys}}}{\text{K}} \right)^{1/2} \times \frac{1\text{T}}{B_0} \times \left(\frac{\text{GeVcm}^{-3}}{\rho_a} \right)^{1/2}, \end{aligned} \quad (3)$$

where SNR is signal to noise ratio, Q is the quality factor, A is cross-sectional area, t is integration time, T_{sys} is the system temperature, B_0 is magnetic field strength and ρ_a is the density of axion dark matter.

In the light of the sensitivity projections in Fig. 2, DALI has a potential to probe DFSZ I-type axion models between 25–50 μeV within approximately four years in the initial phase of the experiment. During phase II, sensitivity will be increased allowing DALI to search for DFSZ I axion in the 50–180 μeV over a period of about ten years.

We recompute the sensitivity of the DALI haloscope by means of Monte Carlo simulations in the Supplemental Material accompanying this letter [96].

B. Other purposes of the DALI project

The detection or parametric constriction of the axion can shed light on a number of problems in physics that are reviewed in the following paragraphs.

1. Examining cosmology in a post-inflationary Universe

The color anomaly is referred to as ‘domain wall number,’ $\mathcal{N} \leftarrow \mathcal{C}$, in cosmology. The moment in the history of the early Universe in which the axion angular field, θ , acquires propagating degrees of freedom is called the ‘phase transition.’ In a scenario in which the phase transition takes place before inflation, axion strings, domain walls, emerging if $\mathcal{N} > 1$, and their remnants, will be cleaned out by the expansion. If symmetry breaking originates after inflation, domain walls would invoke catastrophic topological objects [59, 133, 134]. For axion models which adopt $\mathcal{N} = 1$, such as the KSVZ model, these topological defects are naturally avoided. In a post-inflationary scenario, models with $\mathcal{N} > 1$, including the DFSZ axion, must circumvent those dramatic topologicals by alternative mechanisms [135–140].

Information can be extracted from this picture. The axion mass in a post-inflationary scenario is often restricted to the range $25\text{ }\mu\text{eV} \lesssim m_a \lesssim 1\text{ meV}$ —cf. [30, 59, 141]. Recent studies even constrain this range

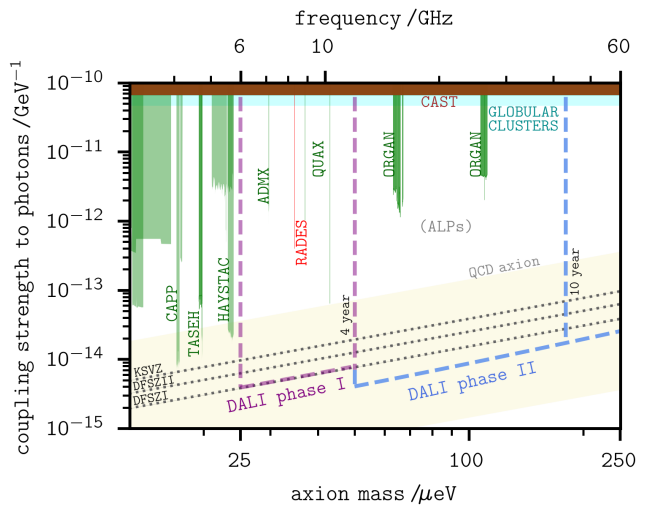


FIG. 2. A forecast of the sensitivity of DALI Experiment to Galactic axion dark matter projected onto current exclusion limits that are differentiated by color [44–58, 70–75, 77, 120–129]. The magnetic field is 9.4 T or 11.7 T for phase I, in purple, and phase II, in blue, respectively. The cross-sectional plate area is $1/2\text{ m}^2$ or $3/2\text{ m}^2$, and about four dozen layers are stacked in series to provide a high quality factor—cf. [96] for details. The system temperature is determined by a subkelvin background temperature provided by ^3He coolers plus an offset contributed by the limit of heat dissipation in the electronics, roughly 2–3 times over the quantum noise limit, in order to be consistent with the frequency-dependent noise figure in high-electron-mobility transistor technology [130, 131] with a physical temperature at the level of one kelvin. This causes a slope with respect to the QCD axion model lines that is partially compensated by a frequency-dependent quality factor. The instantaneous scanning bandwidth is between several dozens to a few hundred megahertz; while the axion-induced signal linewidth is $\Delta\nu/\nu \approx 5 \times 10^{-7}$. The KSVZ and DFSZ axion models are projected over the entire experimental range, 25–250 μeV . The QCD axion window is shaded in yellow [132]. The region in white is compatible with axion-like particles (ALPs).

further, to $40 \lesssim m_a/\mu\text{eV} \lesssim 180$, to which DALI will pay special attention [142].

It is equally appealing that DALI will simultaneously explore the axion mass range constrained by models that unify the strong CP problem, dark matter, usually adopting a KSVZ-type axion, and cosmic inflation, simultaneously solving other problems of modern physics. This band is $50 \lesssim m_a/\mu\text{eV} \lesssim 200$ in order to be compatible with observational data and the ΛCDM cosmology [32–36].

2. Astrophysical bounds of axion dark matter

The confrontation of stellar evolution models, modified to account for the additional energy loss rate that

axion scattering would cause, with observational data, allows to set limits to the coupling constants of the pseudoscalar with ordinary particles. Axion-like particles coupling to both photons and fermions could simultaneously explain both the observed extra cooling in horizontal branch stars, which is compatible with the Primakoff effect, and the abnormally accelerated evolution of red giant branch stars that may originate from axion coupling to electrons in several radiative processes such as atomic axio-recombination or deexcitation, axion bremsstrahlung and Compton scattering. This could also explain additional cooling in white dwarfs through axion-induced losses due to bremsstrahlung; all in concordance with the discrepancy of the neutrino flux duration from supernova (SN) SN1987A compared to simulations, and some intriguing observations of the neutron star in the SN remnant Cassiopeia A that disclose an abnormally fast cooling rate compatible with axion-neutron bremsstrahlung [46, 143–154]. This fosters the exploration of the corresponding mass range with DFSZ axion sensitivity. DALI has a potential to probe these astro-bounds, whose most restrictive limits in its band to date, resulting from observations of globular clusters, are projected onto Fig. 2 [46, 146], with DFSZ I sensitivity.

3. Dark sector photons

Dark photon, also referred to as hidden photon or paraphoton, is a hypothetical gauge boson that mixes kinetically with ordinary photons [62, 63]. The interaction term relevant for this work reads

$$\mathcal{L}_{\gamma'\gamma}^{\text{int}} = -\frac{1}{2} F_{\mu\nu} \tilde{X}^{\mu\nu} \chi, \quad (4)$$

where we denote by $\tilde{X}^{\mu\nu}$ the field strength tensor of the dark photon field; χ being the, dimensionless, kinetic mixing strength.

The sensitivity of DALI to Galactic paraphotons is

$$\begin{aligned} \chi \gtrsim 2.9 \times 10^{-14} \times \left(\frac{\text{SNR}}{Q} \right)^{1/2} \times \left(\frac{m^2}{A} \right)^{1/2} \times \left(\frac{\Delta\nu}{\text{Hz}} \right)^{1/4} \\ \times \left(\frac{1\text{s}}{t} \right)^{1/4} \times \left(\frac{T_{\text{sys}}}{\text{K}} \right)^{1/2} \times \left(\frac{\text{GeVcm}^{-3}}{\rho_{\gamma'}} \right)^{1/2} \times \frac{\sqrt{2/3}}{\alpha}, \end{aligned} \quad (5)$$

$\alpha = \sqrt{2/3}$ representing random incidence angle of the dark photon [167]. Figure 3 shows a forecast of DALI sensitivity considering that hidden photons make up a large part of the Galactic dark matter.

4. Exploration of a dark universe

Different patches, causally disconnected as a result of a scenario at which the phase transition takes place after

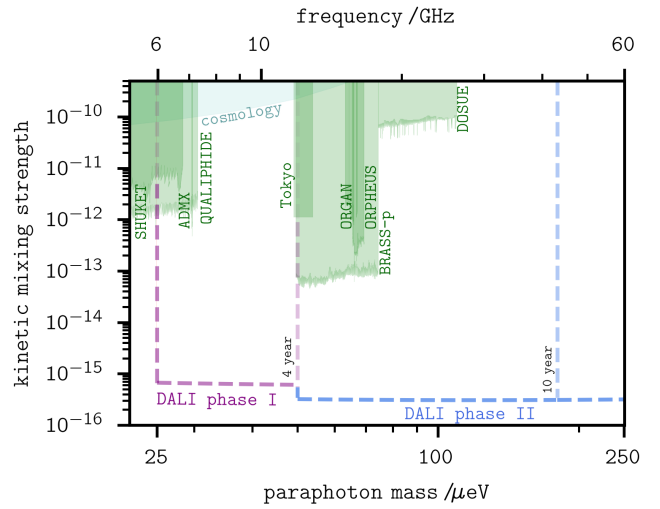


FIG. 3. Projection of the sensitivity of DALI to dark sector photon dark matter with overlapping boundaries published at the time of writing [155–165]. Sensitivity enhancement in a fixed polarisation scenario owing to an unrestricted directionality, as suggested in [166], is not rescaled in this plot.

cosmic inflation, could favour the formation of substructures of axion dark matter [168]. If a substructure were to traverse our planet, it would induce a measurable imprint on the electromagnetic spectrum. Substructures have been shown to approach the Solar System by analyzing survey data, with an event rate that may not be insignificant [169–171]. The daily signal modulation can be expressed in terms of c_0, c_1 and ϕ , in the form $c_0 + c_1 \cos(2\pi t/0.997 + \phi)$; t being the time measured in days from January 1st, and

$$b_0 \cos \lambda_{\text{lab}} - b_1 \sin \lambda_{\text{lab}} \cos(\omega_d t + \phi_{\text{lab}} + \psi), \quad (6a)$$

$$b_1 \cos(\omega_d t + \phi_{\text{lab}} + \psi - \pi), \quad (6b)$$

$$b_0 \sin \lambda_{\text{lab}} + b_1 \cos \lambda_{\text{lab}} \cos(\omega_d t + \phi_{\text{lab}} + \psi), \quad (6c)$$

where $b_0 = \sigma_3 |V_{\text{lab}} - V_a|^{-1}$, $b_1 = (\sigma_1^2 + \sigma_2^2)^{1/2} |V_{\text{lab}} - V_a|^{-1}$, $\psi = \tan^{-1}(\sigma_1/\sigma_2) - 0.721\omega_d - \pi/2$; $\sigma_1 = (-0.055, 0.494, -0.868) \cdot \Upsilon$, $\sigma_2 = (-0.873, -0.445, -0.198) \cdot \Upsilon$, $\sigma_3 = (-0.484, 0.747, 0.456) \cdot \Upsilon$, with $\Upsilon = V_{\odot} + v_{\oplus} \cos(\tau_y)(0.994, 0.109, 0.003) + v_{\oplus} \sin(\tau_y)(-0.052, 0.494, -0.868)$, $\tau_y = 2\pi(t - 79)/365$ [78, 170].

In the particular case of the axion, which has no polarization, the directionality originates along the dimensions in which the detector has a fraction of at least 1/5 of the de Broglie wavelength [170]. DALI incorporates an altazimuth mount which enhances its sensitivity to dark matter flows. This is particularly interesting as DALI is

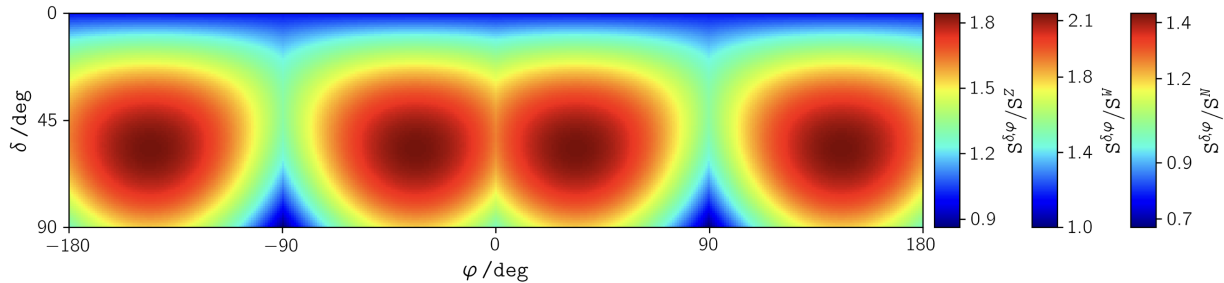


FIG. 4. Significance of the signal modulation, $S^{\delta,\varphi}$, for a collision with a substructure compared to a zenith, north or west pointing experiment, $S^{Z,N,W}$. The inclination angle, δ , is measured from the zenith direction in lab coordinates; and φ is the azimuth angle of its orthogonal projection on a north-west plane measured from the north fixed reference. The optimal pointing varies with lab coordinates, and smoothly over time. This simulation is independent from the axion model and mass and the characteristic properties of the axion flow—density, velocity and dispersion, etc.

envisioned to probe the post-inflationary axion, in a scenario at which topological defects may give rise to substructures. The simulation of an event is shown in Fig. 4. Interestingly, the search for Halo axions and substructures can be performed simultaneously, analyzing the data in parallel. Detection of this trace would support the hypothesis of substructures navigating in a ‘dark universe’ [37–43].

C. Peripheral objectives of the project

1. Probing axion quark nuggets

It has been suggested that the phase transition could concentrate most of the quark excess in the form of invisible quark nuggets, thereby explaining dark matter in the QCD framework [172]. This could give raise to the observed density ratio between non-luminous and visible matter, $\Omega_{\text{dark}}/\Omega_{\text{visible}} \sim 1$. This hypothesis has been transferred to axion [173–178]. Axion quark nuggets (AQNs) are dense relic specks that could arise regardless of the initial misalignment angle or axion mass in a $\mathcal{N} = 1$ scenario. The sensitivity of a DALI-like device to axions released by AQNs is read

$$\frac{g_{a\gamma\gamma}}{\text{GeV}^{-1}} \gtrsim 2.1 \times 10^{-7} \times \left(\frac{\text{SNR}}{Q(v_a)} \right)^{1/2} \times \left(\frac{m^2}{A_s} \right)^{1/2} \times \left(\frac{m_a}{\mu\text{eV}} \right)^{5/4} \times \left(\frac{1\text{s}}{t} \right)^{1/4} \times \left(\frac{T_{\text{sys}}}{\text{K}} \right)^{1/2} \times \frac{1\text{T}}{B_0} \times \left(\frac{\text{eVcm}^{-3}}{\rho_{v_a}^{\text{AQN}}} \right)^{1/2} \times \left(\frac{v_a}{c} \right)^{1/2} \times \frac{1}{\sqrt{n}}. \quad (7)$$

A scaled-down parasitic detector with the same concept as DALI can be devoted to the exploration of the axion flux induced by AQNs on Earth. Such an array of n independent pixels would have a smaller plate scale, s , of the order of a dozen centimeters, in order to maintain de Broglie coherence. This would give the prototype

access to relativistic axions of up to, roughly, one hundred microelectronvolt of mass [78]; with a cut-off close to $c/5$ —note that the spectral density function of AQN-induced axions peaks at about $c/2$. From [176, 177], it follows that the fluence of semi-relativistic axions on Earth originating from collisions with those macroscopic specs is $\Phi_{v_a < c/5}^{\text{AQN}} \sim 10^{12} \text{cm}^{-2}\text{s}^{-1}(\text{eV}/m_a)$, which results in an occupancy of about $\rho_{v_a < c/5}^{\text{AQN}} \sim 10^2 \text{eVcm}^{-3}$. That is several orders of magnitude less concentrated than the saturation density of dark matter at the position of the Solar System, about $\text{few} \times 10^8 \text{eVcm}^{-3}$. However, recent work has pointed out that a gravitationally focused stream of AQNs could transiently increase the occurrence of annihilation events by a factor of up to 10^6 [179]. Notwithstanding that the semi-relativistic velocities of those axions, $v_a \lesssim c/5$, would decrease the signal boost factor [180], a partially resonant, not purely transparent, harmonically hybrid mode could take advantage of the larger momentum transmitted by the rapid axions, allowing to maintain, or perhaps increase, the enhancement factor, $Q(v_a)$, with respect to the low-velocity limit. In addition, signal modulation caused by celestial mechanics, and the so-called ‘local-flashes,’ bursts resulting from the interaction of AQNs with the Earth in the vicinity of a detector, could result in an amplification parameter with magnitude 10^{2-4} during a short period of time with a non-negligible event rate [176, 177]. The sensitivity is multiplied by $[(v_a/c)^2/10^{-6}]^{1/4}$ on the right-hand side of Eq. 7 to give account of the broadening and subsequent dilution of the signal in frequency domain caused by the semi-relativistic velocity of the AQN-induced axions compared to that of virialized particles. However, the above aspects, separately or together, may give the instrument access to the KSVZ axion window.

Eq. 7 can be transferred to any exotic source of semi-relativistic axion astroparticles. One example could be the axion-compatible explanation for the intriguing Antarctic Impulse Transient Antenna events [181–183].

2. Constraints on the diffuse gravitational wave background

Graviton, the gravitational wave (GW) counterpart in the form of a long-postulated elementary particle, mix with photons in the presence of static magnetic fields [66, 184, 185]. The Lagrangian density of the interaction is

$$\mathcal{L}_{g\gamma}^{\text{int}} = -\frac{1}{2}\kappa h_{\mu\nu} B^\mu B^\nu, \quad (8)$$

where the gravitational coupling is $\kappa^2 = 16\pi m_{\text{Pl}}^{-2}$, with $m_{\text{Pl}} \sim 10^{19}$ GeV the Planck mass; $h_{\mu\nu}$ denotes the graviton, B^μ is the external magnetic field and B^ν the electromagnetic wave [186].

Irreducible emission from the time evolution of the momentum-energy tensor and cosmic string decay, the coalescence of primordial black hole (PBH) binaries and the evaporation of low-mass PBHs, branes oscillation, or those of astrophysical origin, such as solar thermal gravitational waves, supernova collapse, rotating neutron stars, binary systems, etc., contribute to shape a diffuse gravitational wave background (GWB) [187–192].

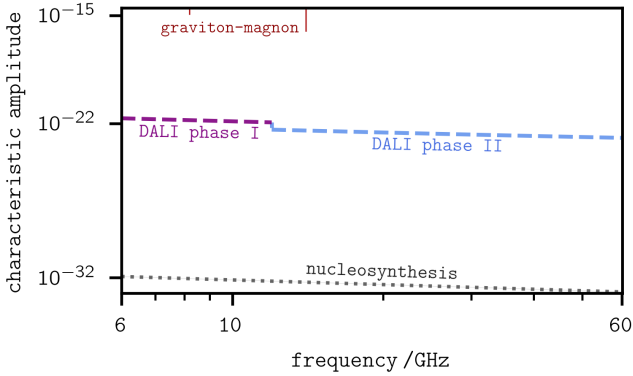


FIG. 5. Accessible characteristic amplitude of a high-frequency stochastic and isotropic gravitational wave background. Results overlapping the experimental range, from [193], are plotted in red.

In the spirit of [188], we now introduce the dimensionless characteristic amplitude $h_c = (6\Omega_{\text{GW}})^{1/2}H_0\omega^{-1}$; with $\Omega_{\text{GW}}(\omega)$ the spectral density function of a stochastic GWB, H_0 the Hubble parameter, ω the pulse of the wave. Primordial gravitational waves contribute to the density of species during nucleosynthesis as massless neutrinos, which results in a higher freezing temperature at which expansion breaks the $pe \leftrightarrow n\nu_e$ equilibrium. This affects the baryon to photon ratio and constraints $h_c \lesssim 4.5 \times 10^{-22} \text{ Hz}/\omega$.

Unfortunately, the cross-section of the photon-graviton oscillation in a magnetic field is weighted by m_{Pl}^{-2} . Therefore, the direct detection of the high-frequency GWB through this approach cannot be tackled with current technology. In any case, some experiments have used the

weak coupling of the graviton to ordinary particles to set bounds to the amplitude of the GWB at shorter wavelengths. Interferometers have established $h_c \gtrsim 10^{-18}$ at 1 MHz, $h_c \gtrsim 10^{-19}$ at 13 MHz and $h_c \gtrsim 10^{-10} - 10^{-12}$ at 100 MHz [194–197]; while the graviton-magnon resonance detector in [193] establishes $h_c \gtrsim 10^{-15}$ at around 8 GHz and $h_c \gtrsim 10^{-16}$ at 14 GHz. The analysis carried out in [192] using data from light-shining-through-walls experiments in [198, 199], and helioscopes [52], establishes the upper bounds $h_c \gtrsim 10^{-25}$ and $h_c \gtrsim 10^{-25}$ at 10^{14-15} Hz, and $h_c \gtrsim 10^{-27}$ at approximately 10^{18} Hz.

DALI may set the most restrictive experimental constraints to the amplitude of the high-frequency GWB in its band via graviton-to-photon conversion in its magnetised vessel. Following the approach in [192, 200], it is possible to infer the minimum amplitude of a stochastic GWB that can be measured by the experiment

$$h_c \gtrsim 9.2 \times 10^{-12} \times \left(\frac{\text{SNR}}{Q}\right)^{1/2} \times \left(\frac{m^2}{A}\right)^{1/2} \times \left(\frac{\text{Hz}}{\nu}\right)^{1/2} \times \left(\frac{1\text{s}}{t}\right)^{1/4} \times \left(\frac{\text{Hz}}{\Delta\nu}\right)^{1/4} \times \left(\frac{T_{\text{sys}}}{K}\right)^{1/2} \times \frac{1\text{T}}{B_0} \times \frac{1\text{m}}{L}, \quad (9)$$

where L is the length of flight. A sensitivity projection is shown in Fig. 5.

IV. CONCLUSIONS

The physics potential of DALI is summarised in Table I. Although the scientific objectives of this experiment are, in some way, puzzling and superimposed, a distinction is attainable. By ramping the magnet on/off it would be possible to differentiate between axion-like and dark photon dark matter. On the other hand, the contribution of nucleosynthesis to an isotropic and stochastic gravitational wave background would manifest itself as a signal that cannot be detuned in small frequency steps. The collision with dark matter substructures would give raise to a peculiar modulation and a shortened signal duration. The spectral feature originated by AQN-induced axions may also have characteristics that would allow it to be discriminated.

ACKNOWLEDGEMENTS

The work of J.D.M. was supported by RIKEN's program for Special Postdoctoral Researchers (SPDR)—Project Code: 202101061013—; J.F.H.C. is supported by the Resident Astrophysicist Programme of the Instituto de Astrofísica de Canarias. We gratefully acknowledge financial support from the Severo Ochoa Program for Technological Projects and Major Surveys 2020-2023 under Grant No. CEX2019-000920-S; Recovery, Transformation and Resiliency Plan of Spanish Government under Grant No. C17.I02.CIENCIA.P5;

TABLE I. Discovery potential of DALI. Recap of the core and peripheral project goals discussed throughout this letter. Axion detection refers to the first third, dark photon physics to the second inset, upper limits to a gravitational wave background follow the last horizontal line. The sensitivity is expressed in terms of $g_{a\gamma\gamma}$ by means of a reference axion model, KSVZ or DFSZ; the kinetic mixing constant, χ , for the paraphoton or the characteristic amplitude of a stochastic gravitational wave background, h_c , for the graviton. The potential impacts of this research are noted.

Branch and purpose	Band	Sensitivity	Impact
Charge&parity (CP) symmetry	25–250 μeV	DFSZ I	Strong CP problem in quantum chromodynamics washed ^a
Galactic axion-like dark matter	25–250 μeV	DFSZ I	Direct detection of dark matter; physics realignment ^b
ΛCDM cosmology (inflation)	40–180 μeV	DFSZ I	Heavier axion sustains cosmic inflation ^c
SMASH-type cosmology	50–200 μeV	>KSVZ	Standard model axion seesaw Higgs portal inflation (SMASH) test ^d
Dark universe (substructures)	25–250 μeV	DFSZ I	Dark matter agglomerates anisotropically in macroscopic structures ^e
Stellar evolution (cooling rate)	25–250 μeV	DFSZ I	Fine-tuning of star model (HB, RGB, WDs, ...) ^f
Axion quark nugget hypothesis	25–80 μeV	KSVZ	Dark matter detection; domain wall number set $\mathcal{N} = 1$ ^g
Dark photon dark matter	25–250 μeV	$\chi \gtrsim 5 \times 10^{-16}$	Dark matter detection; Standard Model of particle physics extends ^h
Gravitational wave background	6–60 GHz	$h_c \gtrsim 10^{-22}$	Bounds to big bang nucleosynthesis by a direct detection method ⁱ

^a Quantum chromodynamics solution to the so-called strong CP problem; a new pseudo-scalar added after the Higgs boson [201–203].

^b If ALPs are found a significant part of dark matter, cosmology and halo modeling, among other issues, may undergo fine adjustment.

^c Observation of axion of mass heavier than several dozens of microelectronvolts would support a post-inflationary scenario.

^d The SMASH window may add three right-handed neutrinos, one Dirac fermion, a new complex singlet scalar [34].

^e Detection of a daily signal modulation can involve large substructures, affecting cosmology, large-scale structure, clusters, galaxies, etc.

^f Confirmation of axion would allow fine-tuning of helium consumption rates; and conversely [46, 146].

^g AQNs set domain wall number, suggests on decay of topologicals, solar ultraviolet radiation excess, ‘primordial lithium puzzle’ [177].

^h If this alternative candidate for dark matter is detected, a dark sector would be added to the Standard Model of particle physics.

ⁱ More incisive experimental limits to the stochastic gravitational wave background provide useful information about the early Universe.

FEDER operational programme under Grant No. EQC2019-006548-P; IAC Plan de Actuación 2022. We thank R. Rebolo, H. Lorenzo-Hernández, R. Hoyland, J. Martín-Camalich, K. Zioutas and A. Zhitnitsky for discussions. This research made use of computing time available on the high-performance computing systems at the Instituto de Astrofísica de Canarias. The authors

thankfully acknowledges the technical expertise and assistance provided by the Spanish Supercomputing Network (Red Española de Supercomputación), as well as the computer resources used: the deimos-diva supercomputer, located at the Instituto de Astrofísica de Canarias.

[1] F. Zwicky, Die Rotverschiebung von extragalaktischen Nebeln, *Helvetica Physica Acta* **6**, 110 (1933).

[2] V. C. Rubin and J. Ford, W. Kent, Rotation of the Andromeda Nebula from a Spectroscopic Survey of Emission Regions, *Astrophys. J.* **159**, 379 (1970).

[3] G. Bertone and D. Hooper, History of dark matter, *Reviews of Modern Physics* **90**, 045002 (2018), arXiv:1605.04909 [astro-ph.CO].

[4] R. H. Dicke, P. J. E. Peebles, P. G. Roll, and D. T. Wilkinson, Cosmic Black-Body Radiation., *Astrophys. J.* **142**, 414 (1965).

[5] A. A. Penzias and R. W. Wilson, A Measurement of Excess Antenna Temperature at 4080 Mc/s., *Astrophys. J.* **142**, 419 (1965).

[6] A. A. Starobinsky, A New Type of Isotropic Cosmological Models Without Singularity, *Phys. Lett. B* **91**, 99 (1980).

[7] A. H. Guth, The Inflationary Universe: A Possible Solution to the Horizon and Flatness Problems, *Phys. Rev. D* **23**, 347 (1981).

[8] A. D. Linde, A New Inflationary Universe Scenario: A Possible Solution of the Horizon, Flatness, Homogeneity, Isotropy and Primordial Monopole Problems, *Phys. Lett. B* **108**, 389 (1982).

[9] A. Albrecht and P. J. Steinhardt, Cosmology for Grand Unified Theories with Radiatively Induced Symmetry Breaking, *Phys. Rev. Lett.* **48**, 1220 (1982).

[10] G. F. Smoot *et al.* (COBE), Structure in the COBE differential microwave radiometer first year maps, *Astrophys. J. Lett.* **396**, L1 (1992).

[11] G. R. Blumenthal, S. Faber, J. R. Primack, and M. J. Rees, Formation of galaxies and large-scale structure with cold dark matter, *Nature* **311**, 517 (1984).

[12] M. Davis, G. Efstathiou, C. S. Frenk, and S. D. White, The evolution of large-scale structure in a universe dominated by cold dark matter, *The Astrophysical Journal* **292**, 371 (1985).

[13] A. Klypin, J. Holtzman, J. Primack, and E. Regos, Structure Formation with Cold plus Hot Dark Matter, *Astrophys. J.* **416**, 1 (1993), arXiv:astro-ph/9305011 [astro-ph].

[14] A. R. Liddle and D. H. Lyth, The cold dark matter density perturbation, *Physics Reports* **231**, 1 (1993).

[15] L. Hernquist, N. Katz, D. H. Weinberg, and J. Miralda-Escude, The lyman-alpha forest in the cold dark matter model, *The Astrophysical Journal* **457**, L51 (1996).

[16] S. Galli, F. Iocco, G. Bertone, and A. Melchiorri, Cmb constraints on dark matter models with large annihilation cross section, *Phys. Rev. D* **80**, 023505 (2009).

[17] W. Hu, Mapping the dark matter through the cosmic microwave background damping tail, *The Astrophysical Journal* **557**, L79 (2001).

[18] D. N. Spergel and P. J. Steinhardt, Observational evidence for self-interacting cold dark matter, *Physical review letters* **84**, 3760 (2000).

[19] W. Hu and S. Dodelson, Cosmic microwave background anisotropies, *Annual Review of Astronomy and Astrophysics* **40**, 171 (2002), <https://doi.org/10.1146/annurev.astro.40.060401.093926>.

[20] S. Alam *et al.* (BOSS), The clustering of galaxies in the completed SDSS-III Baryon Oscillation Spectroscopic Survey: cosmological analysis of the DR12 galaxy sample, *Mon. Not. Roy. Astron. Soc.* **470**, 2617 (2017), arXiv:1607.03155 [astro-ph.CO].

[21] Y. Wang, G.-B. Zhao, C.-H. Chuang, M. Pellejero-Ibanez, C. Zhao, F.-S. Kitaura, and S. Rodriguez-Torres, The clustering of galaxies in the completed SDSS-III Baryon Oscillation Spectroscopic Survey: a tomographic analysis of structure growth and expansion rate from anisotropic galaxy clustering, *Mon. Not. Roy. Astron. Soc.* **481**, 3160 (2018), arXiv:1709.05173 [astro-ph.CO].

[22] N. I. Libeskind *et al.*, Tracing the cosmic web, *Mon. Not. Roy. Astron. Soc.* **473**, 1195 (2018), arXiv:1705.03021 [astro-ph.CO].

[23] Planck Collaboration, Planck 2018 results. VI. Cosmological parameters, *Astronomy & Astrophysics* **641**, A6 (2020), arXiv:1807.06209 [astro-ph.CO].

[24] R. D. Peccei and H. R. Quinn, CP conservation in the presence of pseudoparticles, *Phys. Rev. Lett.* **38**, 1440 (1977).

[25] S. Weinberg, A new light boson?, *Phys. Rev. Lett.* **40**, 223 (1978).

[26] F. Wilczek, Problem of strong p and t invariance in the presence of instantons, *Phys. Rev. Lett.* **40**, 279 (1978).

[27] L. Abbott and P. Sikivie, A cosmological bound on the invisible axion, *Physics Letters B* **120**, 133 (1983).

[28] M. Dine and W. Fischler, The not-so-harmless axion, *Physics Letters B* **120**, 137 (1983).

[29] J. Preskill, M. B. Wise, and F. Wilczek, Cosmology of the invisible axion, *Physics Letters B* **120**, 127 (1983).

[30] Particle Data Group, Review of particle physics, *Phys. Rev. D* **98**, 030001 (2018).

[31] P. Sikivie, Axions, domain walls, and the early universe, *Phys. Rev. Lett.* **48**, 1156 (1982).

[32] A. Salvio, A Simple Motivated Completion of the Standard Model below the Planck Scale: Axions and Right-Handed Neutrinos, *Phys. Lett. B* **743**, 428 (2015), arXiv:1501.03781 [hep-ph].

[33] G. Ballesteros, J. Redondo, A. Ringwald, and C. Tamarit, Standard model—axion—seesaw—higgs portal inflation. five problems of particle physics and cosmology solved in one stroke, *Journal of Cosmology and Astroparticle Physics* **2017** (08), 001.

[34] G. Ballesteros, J. Redondo, A. Ringwald, and C. Tamarit, Unifying inflation with the axion, dark matter, baryogenesis, and the seesaw mechanism, *Physical review letters* **118**, 071802 (2017).

[35] A. Ernst, A. Ringwald, and C. Tamarit, Axion predictions in $so(10) \times u(1)$ pq models, *Journal of High Energy Physics* **2018**, 1 (2018).

[36] G. Ballesteros, J. Redondo, A. Ringwald, and C. Tamarit, Several Problems in Particle Physics and Cosmology Solved in One SMASH, *Frontiers in Astronomy and Space Sciences* **6**, 55 (2019), arXiv:1904.05594 [hep-ph].

[37] C. Hogan and M. Rees, Axion miniclusters, *Physics Letters B* **205**, 228 (1988).

[38] B. Moore, S. Ghigna, F. Governato, G. Lake, T. Quinn, J. Stadel, and P. Tozzi, Dark matter substructure within galactic halos, *The Astrophysical Journal* **524**, L19 (1999).

[39] J. Diemand, M. Kuhlen, P. Madau, M. Zemp, B. Moore, D. Potter, and J. Stadel, Clumps and streams in the local dark matter distribution, *Nature* **454**, 735 (2008).

[40] M. Vogelsberger and S. D. M. White, Streams and caustics: the fine-grained structure of Λ cold dark matter haloes, *Monthly Notices of the Royal Astronomical Society* **413**, 1419 (2011), arXiv:1002.3162 [astro-ph.CO].

[41] P. Tinyakov, I. Tkachev, and K. Zioutas, Tidal streams from axion miniclusters and direct axion searches, *Journal of Cosmology and Astroparticle Physics* **2016** (1), 035, arXiv:1512.02884 [astro-ph.CO].

[42] G. C. Myeong, N. W. Evans, V. Belokurov, N. C. Amorisco, and S. E. Koposov, Halo substructure in the SDSS-Gaia catalogue: streams and clumps, *Monthly Notices of the Royal Astronomical Society* **475**, 1537 (2018), arXiv:1712.04071 [astro-ph.GA].

[43] A. Vaquero, J. Redondo, and J. Stadler, Early seeds of axion miniclusters, *Journal of Cosmology and Astroparticle Physics* **2019** (04), 012.

[44] A. Ayala, I. Dominguez, M. Giannotti, A. Mirizzi, and O. Straniero, Revisiting the Bound on Axion-Photon Coupling from Globular Clusters, *Phys. Rev. Lett.* **113**, 191302 (2014), arXiv:1406.6053 [astro-ph.SR].

[45] O. Straniero, A. Ayala, M. Giannotti, A. Mirizzi, and I. Dominguez, Axion-Photon Coupling: Astrophysical Constraints, in *11th Patras Workshop on Axions, WIMPs and WISPs* (2015) pp. 77–81.

[46] M. J. Dolan, F. J. Hiskens, and R. R. Volkas, Advancing globular cluster constraints on the axion-photon coupling, *Journal of Cosmology and Astroparticle Physics* **2022** (10), 096, arXiv:2207.03102 [hep-ph].

[47] L. Di Luzio, M. Fedele, M. Giannotti, F. Mescia, and E. Nardi, Stellar evolution confronts axion models, *Journal of Cosmology and Astroparticle Physics* **2022** (2), 035, arXiv:2109.10368 [hep-ph].

[48] K. Ehret, M. Frede, S. Ghazaryan, M. Hildebrandt, E.-A. Knabbe, D. Kracht, A. Lindner, J. List, T. Meier, N. Meyer, D. Notz, J. Redondo, A. Ringwald, G. Wiedemann, and B. Willke, New alps results on hidden-sector lightweights, *Physics Letters B* **689**, 149 (2010).

[49] M. Betz, F. Caspers, M. Gasior, M. Thumm, and S. W. Rieger, First results of the cern resonant weakly interacting sub-ev particle search (crows), *Phys. Rev. D* **88**, 075014 (2013).

[50] F. Della Valle, A. Ejlli, U. Gastaldi, G. Messineo, E. Milotti, R. Pengo, G. Ruoso, and G. Zavattini, The PVLAS experiment: measuring vacuum magnetic birefringence and dichroism with a birefringent Fabry-Perot cavity, *European Physical Journal C* **76**, 24 (2016), arXiv:1510.08052 [physics.optics].

[51] R. Ballou, G. Deferne, M. Finger, M. Finger, L. Flekova, J. Hosek, S. Kunc, K. Macuchova, K. A. Meissner,

P. Pugnat, M. Schott, A. Siemko, M. Slunecka, M. Sulc, C. Weinsheimer, and J. Zicha (OSQAR Collaboration), New exclusion limits on scalar and pseudoscalar axion-like particles from light shining through a wall, *Phys. Rev. D* **92**, 092002 (2015).

[52] V. Anastassopoulos *et al.* (CAST), New CAST Limit on the Axion-Photon Interaction, *Nature Phys.* **13**, 584 (2017), arXiv:1705.02290 [hep-ex].

[53] A. Caputo, G. Raffelt, and E. Vitagliano, Muonic boson limits: Supernova redux, *Phys. Rev. D* **105**, 035022 (2022).

[54] K. Hamaguchi, N. Nagata, K. Yanagi, and J. Zheng, Limit on the axion decay constant from the cooling neutron star in cassiopeia a, *Phys. Rev. D* **98**, 103015 (2018).

[55] D. Marsh, H. R. Russell, A. C. Fabian, B. R. McNamara, P. Nulsen, and C. S. Reynolds, A new bound on axion-like particles, *Journal of Cosmology and Astroparticle Physics* **2017** (12), 036.

[56] M. Meyer, M. Giannotti, A. Mirizzi, J. Conrad, and M. A. Sánchez-Conde, Fermi large area telescope as a galactic supernovae axionscope, *Phys. Rev. Lett.* **118**, 011103 (2017).

[57] M. Regis, M. Taoso, D. Vaz, J. Brinchmann, S. L. Zoutendijk, N. F. Bouché, and M. Steinmetz, Searching for light in the darkness: Bounds on alp dark matter with the optical muse-faint survey, *Physics Letters B* **814**, 136075 (2021).

[58] K. M. Backes, D. A. Palken, S. A. Kenany, B. M. Brubaker, S. B. Cahn, A. Droster, G. C. Hilton, S. Ghosh, H. Jackson, S. K. Lamoreaux, A. F. Leder, K. W. Lehnert, S. M. Lewis, M. Malnou, R. H. Maruyama, N. M. Rapidis, M. Simanovskaia, S. Singh, D. H. Speller, I. Urdinaran, L. R. Vale, E. C. van Assendelft, K. van Bibber, and H. Wang, A quantum enhanced search for dark matter axions, *Nature (London)* **590**, 238 (2021), arXiv:2008.01853 [quant-ph].

[59] D. Marsh, Axion cosmology, *Physics Reports* **643**, 1 (2016), axion cosmology.

[60] P. Sikivie, Experimental Tests of the “Invisible” Axion, *Phys. Rev. Lett.* **51**, 1415 (1983).

[61] H. Primakoff, Photoproduction of neutral mesons in nuclear electric fields and the mean life of the neutral meson, *Phys. Rev.* **81**, 899 (1951).

[62] L. B. Okun, Limits of electrodynamics: paraphotons?, *Sov. Phys. JETP* **56**, 502 (1982).

[63] A. Vilenkin, Particles and the universe, G. Lazarides and Q. Shafi (eds.), North Holland, Amsterdam , 133 (1986).

[64] P. Chen, Resonant photon-graviton conversion in EM fields: from earth to heaven, in *1st International Conference on Phenomenology of Unification: from Present to Future* (1994) pp. 379–395.

[65] F. Bastianelli, U. Nucamendi, C. Schubert, and V. M. Villanueva, Photon-graviton mixing in an electromagnetic field, *J. Phys. A* **41**, 164048 (2008), arXiv:0711.0992 [hep-th].

[66] A. D. Dolgov and D. Ejlli, Conversion of relic gravitational waves into photons in cosmological magnetic fields, *JCAP* **12**, 003, arXiv:1211.0500 [gr-qc].

[67] B. P. Abbott *et al.* (LIGO Scientific Collaboration and Virgo Collaboration), Observation of gravitational waves from a binary black hole merger, *Phys. Rev. Lett.* **116**, 061102 (2016).

[68] A. Ejlli, D. Ejlli, A. M. Cruise, G. Pisano, and H. Grote, Upper limits on the amplitude of ultra-high-frequency gravitational waves from graviton to photon conversion, *European Physical Journal C* **79**, 1032 (2019), arXiv:1908.00232 [gr-qc].

[69] T. Fujita, K. Kamada, and Y. Nakai, Gravitational waves from primordial magnetic fields via photon-graviton conversion, *Phys. Rev. D* **102**, 103501 (2020), arXiv:2002.07548 [astro-ph.CO].

[70] S. DePanfilis, A. C. Melissinos, B. E. Moskowitz, J. T. Rogers, Y. K. Semertzidis, W. U. Wuensch, H. J. Halamo, A. G. Prodell, W. B. Fowler, and F. A. Nezrick, Limits on the abundance and coupling of cosmic axions at $4.5 < m_a < 5.0 \mu\text{eV}$, *Phys. Rev. Lett.* **59**, 839 (1987).

[71] C. Hagmann, P. Sikivie, N. S. Sullivan, and D. B. Tanner, Results from a search for cosmic axions, *Phys. Rev. D* **42**, 1297 (1990).

[72] S. J. Asztalos, G. Carosi, C. Hagmann, D. Kimion, K. van Bibber, M. Hotz, L. J. Rosenberg, G. Rybka, J. Hoskins, J. Hwang, P. Sikivie, D. B. Tanner, R. Bradley, and J. Clarke, Squid-based microwave cavity search for dark-matter axions, *Phys. Rev. Lett.* **104**, 041301 (2010).

[73] L. Zhong, S. Al Kenany, K. M. Backes, B. M. Brubaker, S. B. Cahn, G. Carosi, Y. V. Gurevich, W. F. Kindel, S. K. Lamoreaux, K. W. Lehnert, S. M. Lewis, M. Malnou, R. H. Maruyama, D. A. Palken, N. M. Rapidis, J. R. Root, M. Simanovskaia, T. M. Shokair, D. H. Speller, I. Urdinaran, and K. A. van Bibber, Results from phase 1 of the haystac microwave cavity axion experiment, *Phys. Rev. D* **97**, 092001 (2018).

[74] Y. Lee, B. Yang, H. Yoon, M. Ahn, H. Park, B. Min, D. Kim, and J. Yoo, Searching for invisible axion dark matter with an 18 t magnet haloscope, *Phys. Rev. Lett.* **128**, 241805 (2022).

[75] H. Chang, J.-Y. Chang, Y.-C. Chang, Y.-H. Chang, Y.-H. Chang, C.-H. Chen, C.-F. Chen, K.-Y. Chen, Y.-F. Chen, W.-Y. Chiang, W.-C. Chien, H. T. Doan, W.-C. Hung, W. Kuo, S.-B. Lai, H.-W. Liu, M.-W. OuYang, P.-I. Wu, and S.-S. Yu, Taiwan axion search experiment with haloscope: Designs and operations, *Review of Scientific Instruments* **93**, 084501 (2022), <https://doi.org/10.1063/5.0098783>.

[76] I. Stern, A. A. Chisholm, J. Hoskins, P. Sikivie, N. S. Sullivan, D. B. Tanner, G. Carosi, and K. van Bibber, Cavity design for high-frequency axion dark matter detectors, *Rev. Sci. Instrum.* **86**, 123305 (2015), arXiv:1603.06990 [physics.ins-det].

[77] *Exclusion of ALP Cogenesis Dark Matter in a Mass Window Above 100 μeV* (2023) arXiv:2310.00904 [hep-ex].

[78] J. De Miguel, A dark matter telescope probing the 6 to 60 GHz band, *Journal of Cosmology and Astroparticle Physics* **2021** (04), 075.

[79] J. F. Hernández-Cabrera, J. De Miguel, E. Hernández-Suárez, E. Joven-Álvarez, H. Lorenzo-Hernández, C. Otani, M. A. Rapado-Tamarit, and J. A. Rubiño Martín, *Experimental measurement of the quality factor of a Fabry-Pérot open-cavity axion haloscope* (2023) arXiv:2310.16013 [hep-ph].

[80] J. F. H. Cabrera, J. De Miguel, E. J. Álvarez, E. Hernández-Suárez, J. A. Rubiño Martín, and C. Otani, *A forecast of the sensitivity of the DALI Experiment to Galactic axion dark matter* (2023)

arXiv:2310.20437 [hep-ph].

[81] A. Perot and C. Fabry, On the Application of Interference Phenomena to the Solution of Various Problems of Spectroscopy and Metrology, *Astrophys. J.* **9**, 87 (1899).

[82] P. Sikivie, D. B. Tanner, and Y. Wang, Axion detection in the 10^{-4} ev mass range, *Phys. Rev. D* **50**, 4744 (1994).

[83] G. Rybka, A. Wagner, K. Patel, R. Percival, K. Ramos, and A. Brill, Search for dark matter axions with the orpheus experiment, *Phys. Rev. D* **91**, 011701 (2015).

[84] B. Majorovits (MADMAX interest Group), MADMAX: A new road to axion dark matter detection, *J. Phys. Conf. Ser.* **1342**, 012098 (2017), arXiv:1712.01062 [physics.ins-det].

[85] P. Brun *et al.* (MADMAX), A new experimental approach to probe QCD axion dark matter in the mass range above 40 μ eV, *Eur. Phys. J. C* **79**, 186 (2019), arXiv:1901.07401 [physics.ins-det].

[86] M. Baryakhtar, J. Huang, and R. Lasenby, Axion and hidden photon dark matter detection with multilayer optical haloscopes, *Phys. Rev. D* **98**, 035006 (2018).

[87] J. Chiles *et al.*, New Constraints on Dark Photon Dark Matter with Superconducting Nanowire Detectors in an Optical Haloscope, *Phys. Rev. Lett.* **128**, 231802 (2022), arXiv:2110.01582 [hep-ex].

[88] R. Cervantes, G. Carosi, S. Kimes, C. Hannetty, B. H. LaRoque, G. Leum, P. Mohapatra, N. S. Oblath, R. Ottens, Y. Park, G. Rybka, J. Sinnis, and J. Yang, Admx-orpheus first search for 70 μ eV dark photon dark matter: Detailed design, operations, and analysis, *Phys. Rev. D* **106**, 102002 (2022).

[89] R. Cervantes, G. Carosi, C. Hannetty, S. Kimes, B. H. LaRoque, G. Leum, P. Mohapatra, N. S. Oblath, R. Ottens, Y. Park, G. Rybka, J. Sinnis, and J. Yang, Search for 70 μ eV dark photon dark matter with a dielectrically loaded multiwavelength microwave cavity, *Phys. Rev. Lett.* **129**, 201301 (2022).

[90] L. Manenti, U. Mishra, G. Bruno, H. Roberts, P. Oikonomou, R. Pasricha, I. Sarnoff, J. Weston, F. Arneodo, A. Di Giovanni, A. J. Millar, and K. D. Mora, Search for dark photons using a multilayer dielectric haloscope equipped with a single-photon avalanche diode, *Phys. Rev. D* **105**, 052010 (2022).

[91] B. T. McAllister, G. Flower, L. E. Tobar, and M. E. Tobar, Tunable supermode dielectric resonators for axion dark-matter haloscopes, *Phys. Rev. Appl.* **9**, 014028 (2018).

[92] A. P. Quiskamp, B. T. McAllister, G. Rybka, and M. E. Tobar, Dielectric-boosted sensitivity to cylindrical azimuthally varying transverse-magnetic resonant modes in an axion haloscope, *Phys. Rev. Appl.* **14**, 044051 (2020).

[93] K. Renk, *Basics of Laser Physics: For Students of Science and Engineering*, Graduate Texts in Physics (Springer Berlin Heidelberg, 2012).

[94] N. Ismail, C. C. Kores, D. Geskus, and M. Pollnau, Fabry-p#x00e9;rot resonator: spectral line shapes, generic and related airy distributions, linewidths, finesse, and performance at low or frequency-dependent reflectivity, *Opt. Express* **24**, 16366 (2016).

[95] J. F. Hernández-Cabrera, J. De Miguel, E. Hernández-Suárez, E. Joven-Álvarez, H. Lorenzo-Hernández, C. Otani, and J. A. Rubiño Martín, *Free space experimental characterization of a multilayer Fabry-Pérot resonator for DALI* (2023).

[96] See Supplemental Material at [URL will be inserted by publisher] for a numerical estimate of DALI sensitivity by means of a Monte Carlo simulation that shows good agreement with the naive calculation included in the Main Letter (I); and an expanded discussion about the axion-induced signal enhancement tenable in the experiment (II).

[97] S. Hancock, R. D. Davies, A. N. Lasenby, C. M. G. de La Cruz, R. A. Watson, R. Rebolo, and J. E. Beckman, Direct observation of structure in the cosmic microwave background, *Nature (London)* **367**, 333 (1994).

[98] R. A. Watson, P. Carreira, K. Cleary, R. D. Davies, R. J. Davis, C. Dickinson, K. Grainge, C. M. Gutiérrez, M. P. Hobson, M. E. Jones, R. Kneissl, A. Lasenby, K. Maisinger, G. G. Pooley, R. Rebolo, J. A. Rubiño-Martin, B. Rusholme, R. D. E. Saunders, R. Savage, P. F. Scott, A. Slosar, P. J. Sosa Molina, A. C. Taylor, D. Titterington, E. Waldram, and A. Wilkinson, First results from the Very Small Array — I. Observational methods, *Monthly Notices of the Royal Astronomical Society* **341**, 1057 (2003), <https://academic.oup.com/mnras/article-pdf/341/4/1057/3473985/341-4-1057.pdf>.

[99] Planck Collaboration, P. A. R. Ade, N. Aghanim, M. Arnaud, M. Ashdown, J. Aumont, C. Baccigalupi, M. Baker, A. Balbi, A. J. Banday, R. B. Barreiro, J. G. Bartlett, E. Battaner, K. Benabed, K. Bennett, A. Benoît, J. P. Bernard, M. Bersanelli, R. Bhatia, J. J. Bock, A. Bonaldi, J. R. Bond, J. Borrill, F. R. Bouchet, T. Bradshaw, M. Bremer, M. Bucher, C. Burigana, R. C. Butler, P. Cabella, C. M. Cantalupo, B. Cappellini, J. F. Cardoso, R. Carr, M. Casale, A. Catalano, L. Cayón, A. Challinor, A. Chamballu, J. Charra, R. R. Chary, L. Y. Chiang, C. Chiang, P. R. Christensen, D. L. Clements, S. Colombi, F. Couchot, A. Coulais, B. P. Crill, G. Crone, M. Crook, F. Cuttaia, L. Danese, O. D'Arcangelo, R. D. Davies, R. J. Davis, P. de Bernardis, J. de Bruin, G. de Gasperis, A. de Rosa, G. de Zotti, J. Delabrouille, J. M. Delouis, F. X. Désert, J. Dick, C. Dickinson, K. Dolag, H. Dole, S. Donzelli, O. Doré, U. Dörl, M. Douspis, X. Dupac, G. Efstathiou, T. A. Enßlin, H. K. Eriksen, F. Finelli, S. Foley, O. Forni, P. Fosalba, M. Frailis, E. Franceschi, M. Freschi, T. C. Gaier, S. Galeotta, J. Gallegos, B. Gandolfo, K. Ganga, M. Giard, G. Giardino, G. Gienger, Y. Giraud-Héraud, J. González, J. González-Nuevo, K. M. Górski, S. Gratton, A. Gregorio, A. Gruppuso, G. Guyot, J. Haissinski, F. K. Hansen, D. Harrison, G. Helou, S. Henrot-Versillé, C. Hernández-Monteagudo, D. Herranz, S. R. Hildebrandt, E. Hivon, M. Hobson, W. A. Holmes, A. Hornstrup, W. Hovest, R. J. Hoyland, K. M. Huffenberger, A. H. Jaffe, T. Jagemann, W. C. Jones, J. J. Juillet, M. Juvela, P. Kangaslahti, E. Keihänen, R. Keskitalo, T. S. Kisner, R. Kneissl, L. Knox, M. Krassenburg, H. Kurki-Suonio, G. Lagache, A. Lähteenmäki, J. M. Lamarre, A. E. Lange, A. Lasenby, R. J. Laureijs, C. R. Lawrence, S. Leach, J. P. Leahy, R. Leonardi, C. Leroy, P. B. Lilje, M. Linden-Vørnle, M. López-Caniego, S. Lowe, P. M. Lubin, J. F. Macías-Pérez, T. Maciaszek, C. J. MacTavish, B. Maffei, D. Maino, N. Mandolesi, R. Mann, M. Maris, E. Martínez-González, S. Masi, M. Massardi, S. Matarrese, F. Matthai, P. Mazzotta,

A. McDonald, P. McGehee, P. R. Meinhold, A. Melchiorri, J. B. Melin, L. Mendes, A. Mennella, C. Mevi, R. Miniscalco, S. Mitra, M. A. Miville-Deschénes, A. Moneti, L. Montier, G. Morgante, N. Morisset, D. Mortlock, D. Munshi, A. Murphy, P. Naselsky, P. Natoli, C. B. Netterfield, H. U. Nørgaard-Nielsen, F. Noviello, D. Novikov, I. Novikov, I. J. O'Dwyer, I. Ortiz, S. Osborne, P. Osuna, C. A. Oxborrow, F. Pajot, R. Paladini, B. Partridge, F. Pasian, T. Passvogel, G. Patanchon, D. Pearson, T. J. Pearson, O. Perdereau, L. Perotto, F. Perrotta, F. Piacentini, M. Piat, E. Pierpaoli, S. Plaszczynski, P. Platania, E. Pointecouteau, G. Polenta, N. Ponthieu, L. Popa, T. Poutanen, G. Prézeau, S. Prunet, J. L. Puget, J. P. Rachen, W. T. Reach, R. Rebolo, M. Reinecke, J. M. Reix, C. Renault, S. Ricciardi, T. Riller, I. Ristorcelli, G. Rocha, C. Rosset, M. Rowan-Robinson, J. A. Rubiño-Martín, B. Rusholme, E. Salerno, M. Sandri, D. Santos, G. Savini, B. M. Schaefer, D. Scott, M. D. Seiffert, P. Shellard, A. Simonetto, G. F. Smoot, C. Sozzi, J. L. Starck, J. Sternberg, F. Stivoli, V. Stolyarov, R. Stompor, L. Stringhetti, R. Sudiwala, R. Sunyaev, J. F. Sygnet, D. Tapiador, J. A. Tauber, D. Tavagnacco, D. Taylor, L. Terenzi, D. Texier, L. Toffolatti, M. Tomasi, J. P. Torre, M. Tristram, J. Tuovinen, M. Türler, M. Tuttlebee, G. Umana, L. Valenziano, J. Valiviita, J. Varis, L. Vibert, P. Vielva, F. Villa, N. Vittorio, L. A. Wade, B. D. Wandelt, C. Watson, S. D. M. White, M. White, A. Wilkinson, D. Yvon, A. Zacchei, and A. Zonca, Planck early results. I. The Planck mission, *Astronomy and Astrophysics* **536**, A1 (2011), arXiv:1101.2022 [astro-ph.IM].

[100] R. Génova-Santos, J. A. Rubiño-Martín, R. Rebolo, A. Peláez-Santos, C. H. López-Caraballo, S. Harper, R. A. Watson, M. Ashdown, R. B. Barreiro, B. Casappona, C. Dickinson, J. M. Diego, R. Fernández-Cobos, K. J. B. Grainge, C. M. Gutiérrez, D. Herranz, R. Hoyland, A. Lasenby, M. López-Caniego, E. Martínez-González, M. McCulloch, S. Melhuish, L. Piccirillo, Y. C. Perrott, F. Poidevin, N. Razavi-Ghods, P. F. Scott, D. Titterington, D. Tramonte, P. Vielva, and R. Vignaga, QUIJOTE scientific results - I. Measurements of the intensity and polarisation of the anomalous microwave emission in the Perseus molecular complex, *Monthly Notices of the Royal Astronomical Society* **452**, 4169 (2015), arXiv:1501.04491 [astro-ph.GA].

[101] A. J. Millar, G. G. Raffelt, J. Redondo, and F. D. Steffen, Dielectric Haloscopes to Search for Axion Dark Matter: Theoretical Foundations, *JCAP* **01**, 061, arXiv:1612.07057 [hep-ph].

[102] J. R. Costa and J. Guterman, Introduction to antenna and near-field simulation in cst microwave studio software, *IEEE Communication Society, Portugal Chapter* (2010).

[103] J. Mollá, R. Heidinger, A. Ibarra, and G. Link, Dielectric properties of alumina/zirconia composites at millimeter wavelengths, *Journal of Applied Physics* **73**, 7667 (1993), https://pubs.aip.org/aip/jap/article-pdf/73/11/7667/10578995/7667_1_online.pdf.

[104] E. Daw and R. F. Bradley, Effect of high magnetic fields on the noise temperature of a heterostructure field-effect transistor low-noise amplifier, *Journal of Applied Physics* **82**, 1925 (1997), <https://doi.org/10.1063/1.366000>.

[105] R. Bradley, Cryogenic, low-noise, balanced amplifiers for the 300–1200 mhz band using heterostructure field-effect transistors, *Nuclear Physics B - Proceedings Supplements* **72**, 137 (1999), proceedings of the 5th IFT Workshop on Axions.

[106] I. H. Rodrigues, D. Niepce, A. Pourkabirian, G. Moschetti, J. Schleeh, T. Bauch, and J. Grahn, On the angular dependence of inp high electron mobility transistors for cryogenic low noise amplifiers in a magnetic field, *AIP Advances* **9**, 085004 (2019), <https://doi.org/10.1063/1.5107493>.

[107] S. A. Bryan, T. E. Montroy, and J. E. Ruhl, Modeling dielectric half-wave plates for cosmic microwave background polarimetry using a mueller matrix formalism, *Appl. Opt.* **49**, 6313 (2010).

[108] R. Vignaga, *Quijote-mfi optics characterisation and polarisation measurements of cmb foregrounds*, Ph.D. thesis, Instituto de Astrofísica de Canarias, University of La Laguna (2018).

[109] M. D. Bird, I. R. Dixon, and J. Toth, Large, high-field magnet projects at the nwmf, *IEEE Transactions on Applied Superconductivity* **25**, 1 (2015).

[110] H. Liebel, High-field superconducting magnets, in *High-Field MR Imaging*, edited by J. Hennig and O. Speck (Springer Berlin Heidelberg, Berlin, Heidelberg, 2012) pp. 7–25.

[111] Y. Lvovsky, E. W. Stautner, and T. Zhang, Novel technologies and configurations of superconducting magnets for MRI, *Superconductor Science Technology* **26**, 093001 (2013).

[112] C. Abel, S. Afach, N. J. Ayres, C. A. Baker, G. Ban, G. Bison, K. Bodek, V. Bondar, M. Burghoff, E. Chanel, Z. Chowdhuri, P.-J. Chiu, B. Clement, C. B. Crawford, M. Daum, S. Emmenegger, L. Ferraris-Bouchez, M. Fertl, P. Flaux, B. Franke, A. Fratangelo, P. Geltenbort, K. Green, W. C. Griffith, M. van der Grinten, Z. D. Grujić, P. G. Harris, L. Hayen, W. Heil, R. Henneck, V. Hélaine, N. Hild, Z. Hodge, M. Horras, P. Iaydjiev, S. N. Ivanov, M. Kasprzak, Y. Kermadie, K. Kirch, A. Knecht, P. Knowles, H.-C. Koch, P. A. Koss, S. Komposch, A. Kozela, A. Kraft, J. Krempel, M. Kuźniak, B. Lauss, T. Lefort, Y. Lemière, A. Leredde, P. Mohanmurthy, A. Mtchedlishvili, M. Musgrave, O. Naviliat-Cuncic, D. Pais, F. M. Piegsa, E. Pierre, G. Piganiol, C. Plonka-Spehr, P. N. Prashanth, G. Quéméner, M. Rawlik, D. Rebreyend, I. Rienäcker, D. Ries, S. Rocca, G. Rogel, D. Rozpedzik, A. Schnabel, P. Schmidt-Wellenburg, N. Severijns, D. Shiers, R. Tavakoli Dinani, J. A. Thorne, R. Virot, J. Voigt, A. Weis, E. Wursten, G. Wyszynski, J. Zejma, J. Zenner, and G. Zsigmond, Measurement of the permanent electric dipole moment of the neutron, *Phys. Rev. Lett.* **124**, 081803 (2020).

[113] C. A. Baker, D. D. Doyle, P. Geltenbort, K. Green, M. G. D. van der Grinten, P. G. Harris, P. Iaydjiev, S. N. Ivanov, D. J. R. May, J. M. Pendlebury, J. D. Richardson, D. Shiers, and K. F. Smith, Improved experimental limit on the electric dipole moment of the neutron, *Phys. Rev. Lett.* **97**, 131801 (2006).

[114] J. E. Kim, Weak-interaction singlet and strong CP invariance, *Phys. Rev. Lett.* **43**, 103 (1979).

[115] M. A. Shifman, A. Vainshtein, and V. I. Zakharov, Can confinement ensure natural cp invariance of strong interactions, *Nuclear Physics* **166**, 493 (1980).

[116] M. Dine, W. Fischler, and M. Srednicki, A simple solution to the strong cp problem with a harmless axion, *Physics Letters B* **104**, 199 (1981).

[117] A. P. Zhitnitskii, Possible suppression of axion-hadron interactions, *Sov. J. Nucl. Phys. (Engl. Transl.)*; (United States) **31:2**, (1980).

[118] K. Choi, S. H. Im, and C. S. Shin, Recent progress in the physics of axions and axion-like particles, *Annual Review of Nuclear and Particle Science* **71**, 225 (2021), <https://doi.org/10.1146/annurev-nucl-120720-031147>.

[119] F. Chadha-Day, J. Ellis, and D. J. E. Marsh, Axion dark matter: What is it and why now?, *Science Advances* **8**, eabj3618 (2022), <https://www.science.org/doi/pdf/10.1126/sciadv.abj3618>.

[120] A. A. Melcón *et al.* (CAST), First results of the CAST-RADES haloscope search for axions at $34.67 \mu\text{eV}$, *JHEP* **21**, 075, arXiv:2104.13798 [hep-ex].

[121] J. W. Foster, Y. Kahn, O. Macias, Z. Sun, R. P. Eatough, V. I. Kondratiev, W. M. Peters, C. Weniger, and B. R. Safdi, Green Bank and Effelsberg Radio Telescope Searches for Axion Dark Matter Conversion in Neutron Star Magnetospheres, *Phys. Rev. Lett.* **125**, 171301 (2020), arXiv:2004.00011 [astro-ph.CO].

[122] J. Darling, New Limits on Axionic Dark Matter from the Magnetar PSR J1745-2900, *Astrophys. J. Lett.* **900**, L28 (2020), arXiv:2008.11188 [astro-ph.CO].

[123] J. Darling, Search for Axionic Dark Matter Using the Magnetar PSR J1745-2900, *Phys. Rev. Lett.* **125**, 121103 (2020), arXiv:2008.01877 [astro-ph.CO].

[124] C. Boutan, M. Jones, B. H. LaRoque, N. S. Oblath, R. Cervantes, N. Du, N. Force, S. Kimes, R. Ottens, L. J. Rosenberg, G. Rybka, J. Yang, G. Carosi, N. Woollett, D. Bowring, A. S. Chou, R. Khatiwada, A. Sonnenschein, W. Wester, R. Bradley, E. J. Daw, A. Agrawal, A. V. Dixit, J. Clarke, S. R. O'Kelley, N. Crisosto, J. R. Gleason, S. Jois, P. Sikivie, I. Stern, N. S. Sullivan, D. B. Tanner, P. M. Harrington, and E. Lentz (ADMX Collaboration), Piezoelectrically tuned multimode cavity search for axion dark matter, *Phys. Rev. Lett.* **121**, 261302 (2018).

[125] D. Alesini, C. Braggio, G. Carugno, N. Crescini, D. D'Agostino, D. Di Gioacchino, R. Di Vora, P. Falferi, S. Gallo, U. Gambardella, C. Gatti, G. Iannone, G. Lamanna, C. Ligi, A. Lombardi, R. Mezzena, A. Ortolan, R. Pengo, N. Pompeo, A. Rettaroli, G. Ruoso, E. Silva, C. C. Speake, L. Taffarello, and S. Tocci, Galactic axions search with a superconducting resonant cavity, *Phys. Rev. D* **99**, 101101 (2019).

[126] Alesini *et al.*, Search for invisible axion dark matter of mass $m_a = 43 \mu\text{eV}$ with the quax- $a\gamma$ experiment, *Phys. Rev. D* **103**, 102004 (2021).

[127] B. T. McAllister, G. Flower, E. N. Ivanov, M. Goryachev, J. Bourhill, and M. E. Tobar, The organ experiment: An axion haloscope above 15 ghz, *Physics of the Dark Universe* **18**, 67 (2017).

[128] A. Quiskamp, B. T. McAllister, P. Altin, E. N. Ivanov, M. Goryachev, and M. E. Tobar, Direct search for dark matter axions excluding alp co-ogenesis in the 63 to $67 \mu\text{eV}$ range with the organ experiment, *Science Advances* **8**, eabq3765 (2022), <https://www.science.org/doi/pdf/10.1126/sciadv.abq3765>.

[129] C. O'Hare, cajohare/axionlimits: Axionlimits, <https://cajohare.github.io/AxionLimits/> (2020).

[130] M. A. McCulloch, J. Grahn, S. J. Melhuish, P.-A. Nilsson, L. Piccirillo, J. Schleeh, and N. Wade-falk, Dependence of noise temperature on physical temperature for cryogenic low-noise amplifiers, *Journal of Astronomical Telescopes, Instruments, and Systems* **3**, 014003 (2017).

[131] J. Schleeh, J. Mateos, I. Íñiguez-de-la Torre, N. Wade-falk, P. Nilsson, J. Grahn, and A. Minnich, Phonon black-body radiation limit for heat dissipation in electronics, *Nature materials* **14**, 187–192 (2015).

[132] L. Di Luzio, F. Mescia, and E. Nardi, Redefining the Axion Window, *Phys. Rev. Lett.* **118**, 031801 (2017), arXiv:1610.07593 [hep-ph].

[133] A. D. Linde, Axions in inflationary cosmology, *Phys. Lett. B* **259**, 38 (1991).

[134] T. Hiramatsu, M. Kawasaki, K. Saikawa, and T. Sekiguchi, Production of dark matter axions from collapse of string-wall systems, *Phys. Rev. D* **85**, 105020 (2012), [Erratum: *Phys. Rev. D* 86, 089902 (2012)], arXiv:1202.5851 [hep-ph].

[135] S. M. Barr and J. E. Kim, New Confining Force Solution of the QCD Axion Domain-Wall Problem, *Phys. Rev. Lett.* **113**, 241301 (2014), arXiv:1407.4311 [hep-ph].

[136] R. Sato, F. Takahashi, and M. Yamada, Unified origin of axion and monopole dark matter, and solution to the domain-wall problem, *Phys. Rev. D* **98**, 043535 (2018).

[137] A. Ringwald and K. Saikawa, Axion dark matter in the post-inflationary peccei-quinn symmetry breaking scenario, *Phys. Rev. D* **93**, 085031 (2016).

[138] T. Hiramatsu, M. Kawasaki, and K. Saikawa, Evolution of string-wall networks and axionic domain wall problem, *Journal of Cosmology and Astroparticle Physics* **2011** (08), 030.

[139] M. Kawasaki, T. T. Yanagida, and K. Yoshino, Domain wall and isocurvature perturbation problems in axion models, *Journal of Cosmology and Astroparticle Physics* **2013** (11), 030.

[140] K. Harigaya and M. Kawasaki, Qcd axion dark matter from long-lived domain walls during matter domination, *Physics Letters B* **782**, 1 (2018).

[141] C. A. J. O'Hare, G. Pierobon, J. Redondo, and Y. Y. Wong, Simulations of axionlike particles in the postinflationary scenario, *Phys. Rev. D* **105**, 055025 (2022).

[142] M. Buschmann, J. W. Foster, A. Hook, A. Peterson, D. E. Willcox, W. Zhang, and B. R. Safdi, Dark matter from axion strings with adaptive mesh refinement, *Nature Communications* **13**, 1049 (2022), arXiv:2108.05368 [hep-ph].

[143] G. G. Raffelt and D. S. P. Dearborn, Bounds on hadronic axions from stellar evolution, *Phys. Rev. D* **36**, 2211 (1987).

[144] G. G. Raffelt, Particle physics from stars, *Ann. Rev. Nucl. Part. Sci.* **49**, 163 (1999), arXiv:hep-ph/9903472.

[145] N. Viaux, M. Catelan, P. B. Stetson, G. Raffelt, J. Redondo, A. A. R. Valcarce, and A. Weiss, Neutrino and axion bounds from the globular cluster M5 (NGC 5904), *Phys. Rev. Lett.* **111**, 231301 (2013), arXiv:1311.1669 [astro-ph.SR].

[146] A. Ayala, I. Domínguez, M. Giannotti, A. Mirizzi, and O. Straniero, Revisiting the bound on axion-photon coupling from Globular Clusters, *Phys. Rev. Lett.* **113**, 191302 (2014), arXiv:1406.6053 [astro-ph.SR].

[147] M. M. Miller Bertolami, B. E. Melendez, L. G. Althaus, and J. Isern, Revisiting the axion bounds from the Galactic white dwarf luminosity function, *JCAP* **10**,

069, arXiv:1406.7712 [hep-ph].

[148] T. Fischer, S. Chakraborty, M. Giannotti, A. Mirizzi, A. Payez, and A. Ringwald, Probing axions with the neutrino signal from the next galactic supernova, *Phys. Rev. D* **94**, 085012 (2016), arXiv:1605.08780 [astro-ph.HE].

[149] P. Carenza, T. Fischer, M. Giannotti, G. Guo, G. Martínez-Pinedo, and A. Mirizzi, Improved axion emissivity from a supernova via nucleon-nucleon bremsstrahlung, *JCAP* **10** (10), 016, [Erratum: *JCAP* 05, E01 (2020)], arXiv:1906.11844 [hep-ph].

[150] L. B. Leinson, Axion mass limit from observations of the neutron star in Cassiopeia A, *JCAP* **08**, 031, arXiv:1405.6873 [hep-ph].

[151] J. Keller and A. Sedrakian, Axions from cooling compact stars, *Nucl. Phys. A* **897**, 62 (2013), arXiv:1205.6940 [astro-ph.CO].

[152] M. Giannotti, I. G. Irastorza, J. Redondo, A. Ringwald, and K. Saikawa, Stellar Recipes for Axion Hunters, *JCAP* **10**, 010, arXiv:1708.02111 [hep-ph].

[153] O. Straniero, C. Pallanca, E. Dalessandro, I. Dominguez, F. R. Ferraro, M. Giannotti, A. Mirizzi, and L. Piersanti, The RGB tip of galactic globular clusters and the revision of the axion-electron coupling bound, *Astron. Astrophys.* **644**, A166 (2020), arXiv:2010.03833 [astro-ph.SR].

[154] L. D. Luzio, M. Fedele, M. Giannotti, F. Mescia, and E. Nardi, Stellar evolution confronts axion models (2021), arXiv:2109.10368 [hep-ph].

[155] P. Arias, D. Cadamuro, M. Goodsell, J. Jaeckel, J. Redondo, and A. Ringwald, WISPy Cold Dark Matter, *JCAP* **06**, 013, arXiv:1201.5902 [hep-ph].

[156] J. Suzuki, Y. Inoue, T. Horie, and M. Minowa, Hidden photon CDM search at Tokyo, in *11th Patras Workshop on Axions, WIMPs and WISPs* (2015) pp. 145–148, arXiv:1509.00785 [hep-ex].

[157] C. Boutan *et al.* (ADMX), Piezoelectrically Tuned Multimode Cavity Search for Axion Dark Matter, *Phys. Rev. Lett.* **121**, 261302 (2018), arXiv:1901.00920 [hep-ex].

[158] P. Brun, L. Chevalier, and C. Flouzat, Direct Searches for Hidden-Photon Dark Matter with the SHUKET Experiment, *Phys. Rev. Lett.* **122**, 201801 (2019), arXiv:1905.05579 [hep-ex].

[159] A. V. Dixit, S. Chakram, K. He, A. Agrawal, R. K. Naik, D. I. Schuster, and A. Chou, Searching for Dark Matter with a Superconducting Qubit, *Phys. Rev. Lett.* **126**, 141302 (2021), arXiv:2008.12231 [hep-ex].

[160] R. Cervantes *et al.*, ADMX-Orpheus first search for 70 μ eV dark photon dark matter: Detailed design, operations, and analysis, *Phys. Rev. D* **106**, 102002 (2022), arXiv:2204.09475 [hep-ex].

[161] R. Cervantes *et al.*, Search for 70 μ eV Dark Photon Dark Matter with a Dielectrically Loaded Multiwavelength Microwave Cavity, *Phys. Rev. Lett.* **129**, 201301 (2022), arXiv:2204.03818 [hep-ex].

[162] F. Bajjali *et al.*, First results from BRASS-p broadband searches for hidden photon dark matter, *JCAP* **08**, 077, arXiv:2306.05934 [hep-ex].

[163] B. T. McAllister, A. Quiskamp, C. O'Hare, P. Altin, E. Ivanov, M. Goryachev, and M. Tobar, Limits on Dark Photons, Scalars, and Axion-Electromagnetodynamics with The ORGAN Experiment, *Annalen Phys.* **2023**, 2200622 (2022), arXiv:2212.01971 [hep-ph].

[164] S. Kotaka *et al.* (DOSUE-RR), Search for Dark Photon Dark Matter in the Mass Range 74–110 μ eV with a Cryogenic Millimeter-Wave Receiver, *Phys. Rev. Lett.* **130**, 071805 (2023), arXiv:2205.03679 [hep-ex].

[165] K. Ramanathan, N. Klimovich, R. Basu Thakur, B. H. Eom, H. G. Leduc, S. Shu, A. D. Beyer, and P. K. Day, Wideband direct detection constraints on hidden photon dark matter with the qualiphide experiment, *Phys. Rev. Lett.* **130**, 231001 (2023).

[166] A. Caputo, A. J. Millar, C. A. J. O'Hare, and E. Vitagliano, Dark photon limits: A handbook, *Phys. Rev. D* **104**, 095029 (2021), arXiv:2105.04565 [hep-ph].

[167] D. Horns, J. Jaeckel, A. Lindner, A. Lobanov, J. Redondo, and A. Ringwald, Searching for WISPy Cold Dark Matter with a Dish Antenna, *JCAP* **04**, 016, arXiv:1212.2970 [hep-ph].

[168] C. J. Hogan and M. J. Rees, AXION MINICLUSTERS, *Phys. Lett. B* **205**, 228 (1988).

[169] C. A. O'Hare and A. M. Green, Axion astronomy with microwave cavity experiments, *Physical Review D* **95**, 063017 (2017).

[170] S. Knirck, A. J. Millar, C. A. J. O'Hare, J. Redondo, and F. D. Steffen, Directional axion detection, *Journal of Cosmology and Astroparticle Physics* **2018** (11), 051, arXiv:1806.05927 [astro-ph.CO].

[171] C. A. J. O'Hare, C. McCabe, N. W. Evans, G. Myeong, and V. Belokurov, Dark matter hurricane: Measuring the s1 stream with dark matter detectors, *Phys. Rev. D* **98**, 103006 (2018).

[172] E. Witten, Cosmic separation of phases, *Phys. Rev. D* **30**, 272 (1984).

[173] X. Liang and A. Zhitnitsky, Axion field and the quark nugget's formation at the QCD phase transition, *Phys. Rev. D* **94**, 083502 (2016), arXiv:1606.00435 [hep-ph].

[174] H. Fischer, X. Liang, Y. Semertzidis, A. Zhitnitsky, and K. Zioutas, New mechanism producing axions in the AQN model and how the CAST can discover them, *Phys. Rev. D* **98**, 043013 (2018), arXiv:1805.05184 [hep-ph].

[175] X. Liang and A. Zhitnitsky, Gravitationally bound axions and how one can discover them, *Phys. Rev. D* **99**, 023015 (2019), arXiv:1810.00673 [hep-ph].

[176] X. Liang, A. Mead, M. S. R. Siddiqui, L. Van Waerbeke, and A. Zhitnitsky, Axion Quark Nugget Dark Matter: Time Modulations and Amplifications, *Phys. Rev. D* **101**, 043512 (2020), arXiv:1908.04675 [astro-ph.CO].

[177] D. Budker, V. V. Flambaum, X. Liang, and A. Zhitnitsky, Axion Quark Nuggets and how a Global Network can discover them, *Phys. Rev. D* **101**, 043012 (2020), arXiv:1909.09475 [hep-ph].

[178] A. Zhitnitsky, Axion quark nuggets. Dark matter and matter–antimatter asymmetry: Theory, observations and future experiments, *Mod. Phys. Lett. A* **36**, 2130017 (2021), arXiv:2105.08719 [hep-ph].

[179] B. R. Patla, R. J. Nemiroff, D. H. H. Hoffmann, and K. Zioutas, Flux enhancement of slow-moving particles by sun or jupiter: Can they be detected on earth?, *The Astrophysical Journal* **780**, 158 (2013).

[180] A. J. Millar, J. Redondo, and F. D. Steffen, Dielectric haloscopes: sensitivity to the axion dark matter velocity, *JCAP* **10**, 006, [Erratum: *JCAP* 05, E02 (2018)], arXiv:1707.04266 [hep-ph].

[181] P. W. Gorham, J. Nam, A. Romero-Wolf, S. Hoover, P. Allison, O. Banerjee, J. J. Beatty, K. Belov, D. Z.

Besson, W. R. Binns, V. Bugaev, P. Cao, C. Chen, P. Chen, J. M. Clem, A. Connolly, B. Dailey, C. Deaconu, L. Cremonesi, P. F. Dowkontt, M. A. DuVernois, R. C. Field, B. D. Fox, D. Goldstein, J. Gordon, C. Hast, C. L. Hebert, B. Hill, K. Hughes, R. Hupe, M. H. Israel, A. Javaid, J. Kowalski, J. Lam, J. G. Learned, K. M. Liewer, T. C. Liu, J. T. Link, E. Lusczek, S. Matsuno, B. C. Mercurio, C. Miki, P. Miočinović, M. Mottram, K. Mulrey, C. J. Naudet, J. Ng, R. J. Nichol, K. Palladino, B. F. Rauch, K. Reil, J. Roberts, M. Rosen, B. Rotter, J. Russell, L. Ruckman, D. Saltzberg, D. Seckel, H. Schoorlemmer, S. Stafford, J. Stockham, M. Stockham, B. Strutt, K. Tatem, G. S. Varner, A. G. Vieregg, D. Walz, S. A. Wissel, and F. Wu (ANITA Collaboration), Characteristics of four upward-pointing cosmic-ray-like events observed with anita, *Phys. Rev. Lett.* **117**, 071101 (2016).

[182] P. W. Gorham *et al.* (ANITA), Observation of an Unusual Upward-going Cosmic-ray-like Event in the Third Flight of ANITA, *Phys. Rev. Lett.* **121**, 161102 (2018), arXiv:1803.05088 [astro-ph.HE].

[183] I. Esteban, J. Lopez-Pavon, I. Martinez-Soler, and J. Salvado, Looking at the axionic dark sector with ANITA, *Eur. Phys. J. C* **80**, 259 (2020), arXiv:1905.10372 [hep-ph].

[184] M. Gertsenshtein, Resonance of light and gravitational waves, *Soviet Physics JETP. Fiz.* **14**, 84 (1962).

[185] G. Raffelt and L. Stodolsky, Mixing of the photon with low-mass particles, *Phys. Rev. D* **37**, 1237 (1988).

[186] J. A. R. Cembranos, M. C. Diaz, and P. Martin-Moruno, Graviton-photon oscillation in alternative theories of gravity, *Class. Quant. Grav.* **35**, 205008 (2018), arXiv:1806.11020 [gr-qc].

[187] J. A. Marck and J. P. Lasota, eds., *Relativistic gravitation and gravitational radiation. Proceedings, School of Physics, Les Houches, France, September 26-October 6, 1995* (Cambridge Univ.Pr., Cambridge, UK, 1997).

[188] M. Maggiore, Gravitational wave experiments and early universe cosmology, *Phys. Rept.* **331**, 283 (2000), arXiv:gr-qc/9909001.

[189] M. Servin and G. Brodin, Resonant interaction between gravitational waves, electromagnetic waves and plasma flows, *Phys. Rev. D* **68**, 044017 (2003), arXiv:gr-qc/0302039.

[190] G. S. Bisnovatyi-Kogan and V. N. Rudenko, Very high frequency gravitational wave background in the universe, *Class. Quant. Grav.* **21**, 3347 (2004), arXiv:gr-qc/0406089.

[191] C. Clarkson and S. S. Seahra, A gravitational wave window on extra dimensions, *Class. Quant. Grav.* **24**, F33 (2007), arXiv:astro-ph/0610470.

[192] A. Ejlli, D. Ejlli, A. M. Cruise, G. Pisano, and H. Grote, Upper limits on the amplitude of ultra-high-frequency gravitational waves from graviton to photon conversion, *Eur. Phys. J. C* **79**, 1032 (2019), arXiv:1908.00232 [gr-qc].

[193] A. Ito, T. Ikeda, K. Miuchi, and J. Soda, Probing GHz gravitational waves with graviton-magnon resonance, *Eur. Phys. J. C* **80**, 179 (2020), arXiv:1903.04843 [gr-qc].

[194] A. S. Chou, R. Gustafson, C. Hogan, B. Kamai, O. Kwon, R. Lanza, S. L. Larson, L. McCuller, S. S. Meyer, J. Richardson, C. Stoughton, R. Tomlin, R. Weiss, and Holometer Collaboration, MHz gravitational wave constraints with decameter Michelson interferometers, *Phys. Rev. D* **95**, 063002 (2017), arXiv:1611.05560 [astro-ph.IM].

[195] A. M. Cruise and R. M. J. Ingleby, A prototype gravitational wave detector for 100-MHz, *Class. Quant. Grav.* **23**, 6185 (2006).

[196] A. Nishizawa *et al.*, Laser-interferometric Detectors for Gravitational Wave Background at 100 MHz: Detector Design and Sensitivity, *Phys. Rev. D* **77**, 022002 (2008), arXiv:0710.1944 [gr-qc].

[197] T. Akutsu *et al.*, Search for a stochastic background of 100-MHz gravitational waves with laser interferometers, *Phys. Rev. Lett.* **101**, 101101 (2008), arXiv:0803.4094 [gr-qc].

[198] R. Ballou *et al.* (OSQAR), New exclusion limits on scalar and pseudoscalar axionlike particles from light shining through a wall, *Phys. Rev. D* **92**, 092002 (2015), arXiv:1506.08082 [hep-ex].

[199] K. Ehret *et al.*, New ALPS Results on Hidden-Sector Lightweights, *Phys. Lett. B* **689**, 149 (2010), arXiv:1004.1313 [hep-ex].

[200] R. H. Dicke, The measurement of thermal radiation at microwave frequencies, *Review of Scientific Instruments* **17**, 268 (1946), <https://doi.org/10.1063/1.1770483>.

[201] G. Aad *et al.* (ATLAS), Observation of a new particle in the search for the Standard Model Higgs boson with the ATLAS detector at the LHC, *Phys. Lett. B* **716**, 1 (2012), arXiv:1207.7214 [hep-ex].

[202] S. Chatrchyan *et al.* (CMS), Observation of a New Boson at a Mass of 125 GeV with the CMS Experiment at the LHC, *Phys. Lett. B* **716**, 30 (2012), arXiv:1207.7235 [hep-ex].

[203] S. Chatrchyan *et al.* (CMS), Observation of a New Boson with Mass Near 125 GeV in pp Collisions at $\sqrt{s} = 7$ and 8 TeV, *JHEP* **06**, 081, arXiv:1303.4571 [hep-ex].

[204] B. M. Brubaker, L. Zhong, S. K. Lamoreaux, K. W. Lehnert, and K. A. van Bibber, HAYSTAC axion search analysis procedure, *Phys. Rev. D* **96**, 123008 (2017).

[205] X. Zhao and D. Vanderbilt, Phonons and lattice dielectric properties of zirconia, *Phys. Rev. B* **65**, 075105 (2002).

[206] G.-M. Rignanese, F. Detraux, X. Gonze, and A. Pasquarello, First-principles study of dynamical and dielectric properties of tetragonal zirconia, *Phys. Rev. B* **64**, 134301 (2001).

[207] P. S. André, L. C. Costa, and S. Devesa, Fabry–perot-based approach for the measurement of complex permittivity of samples inserted in resonant cavities, *Microwave and Optical Technology Letters* **43**, 106 (2004), <https://onlinelibrary.wiley.com/doi/pdf/10.1002/mop.20390>.

[208] M. Lanagan, J. Yamamoto, A. Bhalla, and S. Sankar, The dielectric properties of yttria-stabilized zirconia, *Materials Letters* **7**, 437 (1989).

[209] F. A. Miranda, W. L. Gordon, V. O. Heinen, B. T. Ebihara, and K. B. Bhasin, Measurements of complex permittivity of microwave substrates in the 20 to 300 k temperature range from 26.5 to 40.0 ghz, in *Advances in Cryogenic Engineering: Part A & B*, edited by R. W. Fast (Springer US, Boston, MA, 1990) pp. 1593–1599.

Discovery prospects with the Dark-photons & Axion-Like particles Interferometer

Supplementary Material

Javier De Miguel, Juan F. Hernández-Cabrera, Elvio Hernández-Suárez, Enrique Joven-Álvarez, Chiko Otani, and J. Alberto Rubiño-Martín

I. ON THE SENSITIVITY PROJECTION TO GALACTIC AXIONS

In this supplementary material we recompute the sensitivity of DALI to Galactic axion dark matter by means of a Monte Carlo simulation, for which we will mainly follow [128, 204]. The input data consists of M individual spectra containing 2^N bins each generated synthetically. First, an average baseline is estimated by applying a Savitzky–Golay (SG) filter with a window size $W = 3001$ and a polynomial degree $d = 2$ to the average of all spectra. The average spectrum is then divided by the estimated baseline. Bins potentially compromised by intermediate frequency (IF) interferences are identified as any bin deviating more than 4.5σ from the average as well as 3 bins to each side; the values of these bins are iteratively replaced by randomly generated values drawn from a Gaussian distribution with the same average and standard deviation as the values of the average spectrum until no further compromised bins are identified. The corresponding bins of the individual spectra are also replaced with random values in the same manner. Bins potentially compromised by spurious radio frequency (RF) interference are identified in individual spectra as any bin deviating more than several sigma from the average, the threshold being an arbitrary value that is established based on the exclusion sector to be considered. Their values are iteratively replaced by randomly generated values drawn from a Gaussian distribution until no further RF interferences are found. The spectra are individually normalised to their estimated baseline, which is obtained by means of a SG filter with the same parameters as before, to get the processed spectra. Processed spectra are now rescaled by the expected power boost at each frequency to calculate the rescaled spectra, namely

$$\delta_{ij}^s = \frac{\delta_{ij}^p}{Q_{ij}}, \quad (S1)$$

where δ is the value of a bin, i is the index of a spectrum among all spectra, j is the index of a bin within a spectrum and Q_{ij} is the power boost provided by the resonator at each bin. The superscripts s and p represent the rescaled and the processed spectra, respectively. The standard deviation of each bin is given by

$$\sigma_{ij}^s = \frac{\sigma_i^p}{Q_{ij}}. \quad (S2)$$

The rescaled spectra are then combined into a stacked spectrum. The RF bins corresponding to a single IF bin—i.e., non-overlapping bands—are copied directly onto the stacked spectrum; RF bins in overlapping bands are combined by means of a maximum likelihood (ML) weighted sum where the weights w_{ijk} are calculated as

$$w_{ijk} = \frac{(\sigma_{ij}^s)^{-2}}{\sum_{i'} \sum_{j'} (\sigma_{i'j'}^s)^{-2}}, \quad (S3)$$

where k is the index of the stacked spectrum. The prime notation in the denominator is to be interpreted as a sum across all pairs i, j corresponding to a bin k . The stacked spectrum can then be processed as

$$\delta_k^c = \sum_{i'} \sum_{j'} w_{ijk} \delta_{ij}^s \quad (S4)$$

in the overlapping bands. The standard deviation of each stacked spectrum bin is calculated as

$$\sigma_k^c = \sqrt{\sum_{i'} \sum_{j'} w_{ijk}^2 (\delta_{ij}^s)^2}. \quad (S5)$$

Now the rebinned spectrum is obtained by merging neighbouring bins of the stacked spectrum in non-overlapping segments of a length equal to K_r bins. Let $D_k^c = \delta_k^c (\sigma_k^c)^{-2}$ and $R_k^c = (\sigma_k^c)^{-1}$. The rebinned spectrum is obtained from

$$D_\ell^r = \sum_{k=(\ell-1)K_r+1}^{k=\ell K_r} D_k^c \quad (S6)$$

and

$$R_\ell^r = \sqrt{\sum_{k=(\ell-1)K_r+1}^{k=\ell K_r} (D_k^c)^2}, \quad (S7)$$

where ℓ is the index of the rebinned spectrum. The grand spectrum is obtained from a ML weighted sum taking into account the expected power spectral density or line shape $S_a(\nu)$ of the axion-induced signal. In this implementation, we have considered

$$S_a(\nu) = K \sqrt{\nu - \nu_a} \exp\left(-\frac{3(\nu - \nu_a)}{\nu_a \frac{\langle v_a^2 \rangle}{c^2}}\right), \quad (S8)$$

at which K is a constant added to scale $S_a(\nu)$ to its expected power. The weights are calculated by integrating over segments of $S_a(\nu)$ with a length of K_r bins given a misalignment $\delta\nu_r$, according to

$$L_q(\delta\nu_r) = K_g \int_{\nu_a + \delta\nu_r + (q-1)K_r \Delta\nu_b}^{\nu_a + \delta\nu_r + qK_r \Delta\nu_b} S_a(\nu) d\nu, \quad (S9)$$

where q is an index running from 1 up to K_g —the length of the grand spectrum ML sum—and $\Delta\nu_b$ is the bin width of the original spectra. It should be noted that the lengths K_r and K_g must be chosen such that the axion width, $\Delta\nu$, is, approximately, $K_r K_g$ bins wide. The spectral density function $S_a(\nu)$ has a full width half maximum of about $5 \times 10^{-7} \nu_a$ if a value of $(270 \text{ km/s})^2$ is considered for $\langle v_a^2 \rangle$ in a Maxwell–Boltzmann distribution [204]. In this procedure, we have considered an axion width equal to ~ 1.5 times the full width half maximum of $S_a(\nu)$. The misalignment is defined over a range given by

$$-z K_r \Delta\nu_b \leq \delta\nu_r \leq (1-z) K_r \Delta\nu_b \quad (S10)$$

for $0 \leq z \leq 1$. The value of z must be set such that the sum $\sum_q L_q / K_g$ yields a larger value than the one obtained if the sum limits were shifted by 1 up or down for all $\delta\nu_r$. The weights \bar{L}_q are obtained by averaging out $L_q(\delta\nu_r)$ over the range of $\delta\nu_r$. The grand spectrum is now calculated as

$$D_\ell^g = \sum_q D_{\ell+q-1}^r \bar{L}_q, \quad (S11)$$

and

$$R_\ell^g = \sqrt{\sum_q (D_{\ell+q-1}^r \bar{L}_q)^2}. \quad (S12)$$

The normalised spectrum is obtained as $\delta_\ell^g / \sigma_\ell^g = D_\ell^g / R_\ell^g$. In order to account for filter-induced correlations among bins, the standard deviation, ξ , of the normalised grand spectrum is calculated, from which a corrected grand spectrum standard deviation $\tilde{\sigma}_\ell^g = \sigma_\ell^g / \xi$ is obtained. The output of this method, which is the normalised and corrected grand spectrum, is calculated as $\delta_\ell^g / \tilde{\sigma}_\ell^g$. An exclusion sector determined by the bins exceeding a threshold Θ for an arbitrary confidence level (CL) can be established, $\Theta = \text{SNR} - \Phi^{-1}(\text{CL})$, Φ being the cumulative distribution function of the standard normal distribution.

In Fig. S1, we report the result of a simulation after calculating 10,000 iterations. In each iteration, raw bins have been generated as random numbers in each spectrum drawn from a Gaussian distribution with mean $\mu = k_B T_{\text{sys}} \Delta\nu_b$ and deviation $\sigma = k_B T_{\text{sys}} \Delta\nu_b / \sqrt{t \Delta\nu_b}$ [200], scaled by the power boost curve [78]. An artificially generated discrete axion-induced signal has been inserted to one of the spectra as $S_{a,ij} \approx \Delta\nu_b S_a(\nu_{ij})$, which is successfully flagged. The resulting spectra are introduced as an input to the analysis procedure and the value of the output in a window of 150 bins at each side of the bin where the axion signal was inserted has been recorded. An instantaneous scanning bandwidth of 50 MHz has been considered, effective integration time is set to five days per subspectrum, and an array size of 2^{18} has been considered resulting in a bin width $\Delta\nu_b \simeq 190.7 \text{ Hz}$. A total of $M = 2$ spectra with an overlap of 5 MHz have been considered around a central frequency of about 24.2 GHz, where the synthetic axion signal has been injected with $g_{a\gamma\gamma} \simeq 1.5 \times 10^{-14} \text{ GeV}^{-1}$, which corresponds to a DFSZ I axion of 100 μeV mass. Since an axion width of approximately 90 bins is expected at this frequency, $K_r = 7$ and $K_g = 14$ have been considered, for which the value $z = 0.51$ has been numerically found to best fit the requirements in Eq. S11 and Eq. S12. The weights, \bar{L}_q , have been calculated for $\nu_a \simeq 24.2 \text{ GHz}$, but any frequency in the scan range would be suitable given that variations of $S_a(\nu)$ along a series of M subspectra tend to be negligible.

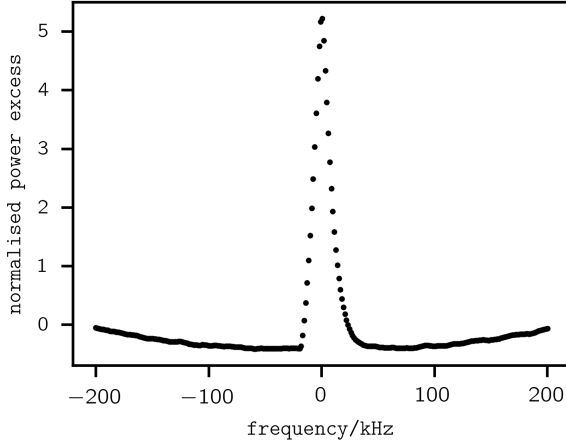


FIG. S1. Sensitivity calculation. The average value of the normalised corrected grand spectrum, $\delta_\ell^g / \tilde{\sigma}_\ell^g$, in a window of 150 bins to each side of the frequency where a synthetic axion signal has been injected is represented. The peak value (5.217) is to be interpreted as the SNR of the axion-induced signal. The distributions of the values of all bins of the analysed window have a standard deviation close to 1. The ripple around the peak is an artifact of the filtering. The abscissa axis has been scaled by K_r to account for the rebinning.

II. ON THE QUALITY FACTOR AND THE ONE-EIGHTH WAVELENGTH PLATE STACK

In this material we explore the quality factor (Q) tenable in a dielectric Fabry–Pérot axion haloscope in practice, for which we put together the experimental results in [79, 95]. The devices under test (DUTs) are two similar fixed-plate Fabry–Pérot resonators with $N = 2, \dots, 5$ layers of dimensions $100 \times 100 \pm 0.5$ mm size and 1 ± 0.03 mm thickness each. The ceramic used is 3 mol% yttria stabilized tetragonal zirconia [205, 206] polycrystal (3Y-TZP) aquired to SITUS Technicals GmbH. The surface roughness of the zirconia wafers is < 0.1 μm . Dielectric losses of this material are of the order of $\tan \delta \sim 10^{-4}$ at $\mathcal{O}(10)$ GHz frequencies [103]. The value of the dielectric constant of this substrate obtained in our laboratory following the method in André *et al.* [207] turns out to be unusually low with respect to the typical permittivity of tetragonal zirconia (t-ZrO₂) measured for a range of different compositions—in particular, $\varepsilon_r \sim 10 - 14$ (measured) versus $\varepsilon_r \sim 30 - 46$ [103, 208, 209]. Since the peak of the Lorentzian spectral feature of the quality factor scales with the permittivity of the dielectric boundary [93], this commensurated the observed Q by a factor of a few, although it does allow us to perform a proof of concept, including the experimental test of the one-eighth wavelength principle. In this concern, two different plate holders were manufactured in aluminum with an error of about three dozen microns or less, according to metrology data. The plate distance is 6.04 mm for DUT 1 and 6.21 mm for DUT 2 in order to resonate at frequencies $\sim 1/2$ GHz apart. For each plate distance, 6.04 mm or 6.21 mm, the spacing is, simultaneously, a fraction of the scanning wavelength of $\sim \lambda/8$ for a one-eighth wavelength stack, to be tested in low frequency measurements, and $\sim \lambda/2$ for a half-wavelength configuration.

Both DUTs were tested at low and high frequency at room temperature. The alignment of the optical setup has an accuracy of $\lesssim 1^\circ$. A vector network analyzer (VNA) is used to acquire the scattering parameters. Free-space measurement between two antennas are taken as a reference. Time domain data gating allows spurious reflections to be filtered out, surfacing the performance of each Fabry–Pérot resonator. When a flat copper mirror is inserted after the last plate maintaining the same spacing with it to maintain phase coherence, the reflection coefficient is measured and the group delay time of the photons through a DUT is estimated. The quality factor is computed as $Q = -\omega d\phi/d\omega$, ϕ being the phase [93, 94]. A schema of the minimum assembly is shown in Fig. S2.

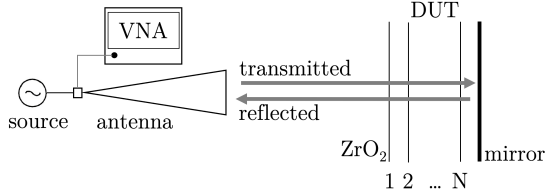


FIG. S2. Schematic setup used for the measurement of the quality factor of DUT1 and DUT2 at low and high frequency.

The experiment results are shown in Fig. S3 [79, 95]. Inside each DUT, the incident wave and the reflected wave interfere coherently at both one-eighth and one-half of the scanning wavelength simultaneously, unveiling the power spectral density of the autocorrelation function at two different resonant frequencies that are approximately four wavelengths apart. In particular, the resonant feature peaks at about 7 and 33 GHz—in both DUTs, with the aforementioned relative shift. This is consistent with a periodic resonance over $\sim 4\nu_0$ intervals once deviations with respect to an ideal plate thickness of $\sim \lambda/(8\sqrt{\varepsilon_r})$ or $\sim \lambda/(2\sqrt{\varepsilon_r})$ caused by the fixed plate thickness of 1 mm are considered.

From the inference that the quality factor scales linearly with the number of plates in series up to a relatively large number of layers [101], we estimate a maximum quality factor of $Q \gtrsim 10^4$ for a Fabry–Pérot axion haloscope with $N \sim 40$ –50 with this particular 3Y-TZP composition. Nevertheless, different t-ZrO₂ wafers with a different structure and composition provide a higher dielectric constant, of the order of $\varepsilon_r \gtrsim 40$ [103]. The quality factor for these substrates would scale up to $Q \gtrsim 50,000$ at ~ 60 GHz for a stack of ~ 50 layers, even including here dielectric losses and a decrease of the dielectric constant observed at cryogenic temperatures [209]. Therefore, we are preparing to carry out further tests on a series of t-ZrO₂ ceramic substrates with better dielectric properties procured from various sources. This will allow us to determine the specific zirconia composition to be incorporated into DALI.

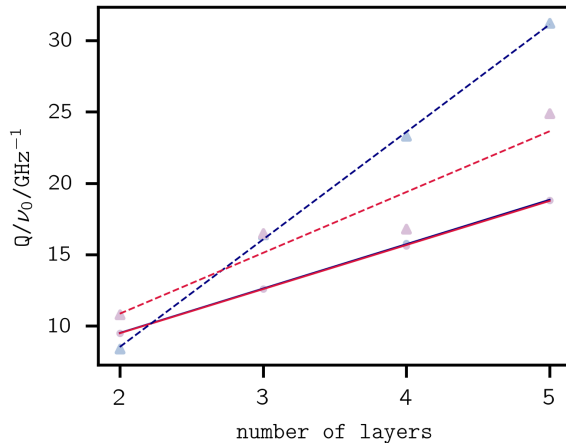


FIG. S3. Experimental measurements of the quality factor for a stack of N plates of 3 mol% yttria stabilized tetragonal zirconia of 100x100x1 mm each. Two twin fixed-plate resonators were fabricated and tested with a frequency shift between them. The results for DUT 1 are shown in blue and those of DUT 2 in red. The circular points were taken at low frequency (~ 7 GHz) and the triangular points are at high frequency (~ 33 GHz). At high and low frequency, where diffraction can play a role since the plate size is of the order of the wavelength, different equipment is used. We normalize the observed quality factor to the resonant frequency to evidence the one-eight wavelength concept. The lines are the least squares fits.